RESEARCH



Parameter identification in non-smooth gap systems with an improved spherical simplex-radial cubature quadrature kalman filter and strong tracking techniques

Jipeng Yang · Jianting Zhou · Hong Zhang · Mingming Song · Xiaoming Lei

Received: 17 April 2025/Revised: 2 September 2025/Accepted: 15 September 2025/Published online: 10 October 2025 © The Author(s) 2025

Abstract Accurate parameter identification is critical for the effective modeling and control of dynamic systems, especially those exhibiting complex, nonlinear behaviors such as non-smooth gap systems. These systems, characterized by abrupt changes in dynamics due to physical constraints, discontinuities, or contact phenomena, pose significant challenges for traditional parameter identification methods, often resulting in inaccurate models and suboptimal system performance. To address these challenges, this study introduces the Strong Tracking Square Root Spherical Simplex-Radial Cubature Quadrature Kalman Filter (STSR-SSRCQKF), an advanced filtering algorithm designed to enhance parameter identification accuracy in non-smooth gap systems. The STSR-SSRCQKF provides several key benefits, including improved numerical stability through the adoption of QR decomposition, which avoids the need for positivedefinite matrices, rapid adaptation to sudden system changes via strong tracking techniques, increased accuracy through a two-fold increase in sampling points, and computational simulations by utilizing acceleration data for alignment with commonly available measurements. The effectiveness of this method is validated on both 1-DoF and 5-DoF nonsmooth systems. Through extensive simulations and comparisons under varying noise levels, large initial errors and limited measurement, the proposed approach demonstrates good performance. The capability of the STSR-SSRCQKF to accurately identify unknown switching points and ensure reliable state tracking in complex, non-smooth systems highlight its potential for broader applications in structural health monitoring, robotics, and dynamic system analysis.

Keywords System identification · Gap systems · Kalman filter · Strong tracking · Non-smooth system · Geometric nonlinearity

J. Yang · J. Zhou · H. Zhang School of Civil Engineering, Chongqing Jiaotong University, Chongqing 400074, China

M. Song Department of Bridge Engineering, Tongji University, Shanghai 200092, China

X. Lei ((\infty))
Department of Civil and Environmental Engineering,
The Hong Kong Polytechnic University,
Hong Kong SAR 900273, China
e-mail: leixiaoming@outlook.com;
xiaoming.lei@polyu.edu.hk

1 Introduction

Parameter identification is essential in the modeling and control of dynamic systems, especially those with complex and nonlinear behaviors [1]. Non-smooth gap systems, which feature abrupt changes in dynamics due to physical constraints, discontinuities, or contact phenomena, are particularly challenging to model and



analyze [2]. These systems are common in engineering applications, such as dynamics change rapidly upon contact, robotics with joint friction, and structural systems subject to sudden load changes [3]. The inherent non-smoothness of these systems often complicates the accurate estimation of their parameters, which is essential for precise control and reliable performance [4]. Moreover, traditional parameter identification methods frequently struggle to capture the intricate dynamics of non-smooth gap systems, resulting in inaccurate models and suboptimal system performance.

System identification involves developing mathematical models of dynamic systems based on observed data [5]. Time-frequency methods like the Hilbert-Huang Transform (HHT) and wavelet transform (WT) decompose vibration signals into the time-frequency domain and can yield impressive results [6, 7]. However, these methods are not suitable for online identification of structural parameters [8, 9]. For online parameter identification, time-domain methods are more commonly employed [10, 11]. Traditional time-domain system identification techniques, such as least squares estimation, maximum likelihood estimation, and classical Kalman Filter (KF), are wellestablished for linear systems, but they encounter significant challenges when applied to nonlinear and non-smooth systems [12].

The Extended Kalman Filter (EKF) is a widely used algorithm that extends the classical KF to handle nonlinear systems by linearizing the system dynamics around the current estimate [13, 14]. Li and Wang [15] developed a constrained EKF to accurately estimate the parameters of the Bouc-Wen hysteretic model. Zhang et al. [16] introduced a two-stage framework that combines an adaptive EKF with a recursive leastsquares method to track structural parameters and restoring forces in cable-bracing inerter systems. Furthermore, Zhang et al. [17] applied an adaptive EKF to identify time-variant parameters and mass distribution from limited observations. A key disadvantage of the EKF is its reliance on linearization, which can lead to inaccuracies and instability in highly nonlinear systems.

Unscented Kalman Filter (UKF) is another online nonlinear system identification method [18, 19]. The EKF linearizes the system around the current estimate, while the UKF uses a deterministic sampling approach to capture the nonlinearities [20, 21]. Wang and Lei

[22] developed a UKF designed to handle unknown inputs for real-time joint input and system identification of structural systems, particularly in scenarios without direct feedthrough and using limited response measurements. Yu et al. [23] introduced an iterative augmented UKF for simultaneous estimation of state, parameters, and inputs, which adheres to Bayes' theorem without relying on ad hoc procedures, thus offering theoretical simplicity. Additionally, Yuen et al. [24] proposed a Bayesian probabilistic algorithm that integrates UKF for noise covariance estimation, suitable for nonstationary conditions. The chosen sigma points may fail to represent system dynamics accurately, particularly in regions where the system exhibits discontinuities, which can pose challenges for both UKF and EKF in handling highly nonlinear or non-smooth systems.

The Cubature Kalman Filter (CKF) [25, 26] and its extension, the Cubature Quadrature Kalman Filter (CQKF), have been developed to address some of these limitations [27]. These use higher-order statistical moments and cubature integration to provide more accurate estimates for nonlinear systems. Ghorbani and Cha [28] proposed an enhanced UKF that integrates CKF techniques to improve system identification performance in systems with significant degrees of freedom (DoF). Basetti et al. [29] introduced a derivative-free method utilizing Square-Root CKF (SR-CKF) for tracking power system dynamics and providing real-time updates on system state evolution. Mu et al. [30] developed fractional embedded CKF and robust fractional embedded CKF to estimate states in fractional-order nonlinear discrete systems. However, in the context of non-smooth gap systems, even the CQKF can face challenges due to sudden changes in system dynamics.

With different rules for generating sigma points, current sigma point sampling strategies mainly include symmetric sampling, simplex sampling, third-order moment skewness sampling, and fourth-order moment symmetric sampling based on Gaussian distribution, among which symmetric sampling is commonly used. The UKF is the most widely applied and features 2n+1 sigma points. When performing parameter identification, the UKF requires some parameters to be manually defined, which can significantly influence the identification results. This method typically achieves third-order accuracy. The CKF decomposes difficult integrations into surface



and radial integrals on a sphere, approximated using the third-order cubature rule. CKF has 2n equally weighted cubature points (or sigma points) and, unlike the UKF, does not require additional parameter definitions, with its weight values only depending on the dimension of the state vector. This method also generally provides third-order accuracy [31]. The Spherical Simplex Radial Cubature Quadrature Kalman Filter (SSRCQKF) replaces spherical integration with spherical simplex radial cubature quadrature, offering higher accuracy. This paper selects a sampling method with fifth-order accuracy, which results in 4n + 4 sigma points for an *n*-dimensional state vector. Although this method is more computationally intensive, it typically yields better identification performance [32]. Furthermore, traditional KF algorithms typically use Cholesky decomposition to calculate the square root of the covariance matrix during the recursive process in generating sigma points. This requires the covariance matrix to be positive definite [33].

Non-smooth systems are characterized by abrupt changes in dynamics, often resulting from discontinuities, impacts, or constraints in the system [34, 35]. Research in non-smooth systems has led to the development of specialized modeling techniques, such as differential inclusions and complementarity problems, which are designed to handle discontinuities and non-differentiable behaviors [36, 37]. However, these approaches often result in complex models that are difficult to analyze and simulate, especially when it comes to parameter identification.

Modeling non-smooth gap systems presents a significant challenge due to their inherent discontinuities [38, 39]. Traditional parameter identification methods, typically developed for smooth and continuous systems, often rely on assumptions that fail in non-smooth contexts. To address these limitations. several modified methods based on the traditional KF have been proposed. Chatzis et al. [40] introduced a discontinuous EKF (DEKF) specifically for nonsmooth dynamic problems, designed to prevent the temporary divergence and ultimate failure often seen with standard EKF in accurately identifying system parameters. Zhou et al. [41] developed a non-smooth observer that estimates errors in a switched system by incorporating extended disturbances and carefully selecting feedback matrices, enabling accurate state estimation in non-smooth sandwich systems with hysteresis. Zhu et al. [42] proposed a discontinuous UKF (DUKF) featuring a dynamic boundary approximation algorithm to identify state transitions and coupled internal mechanical and geometric parameters. These studies collectively showcase the effectiveness of geometric-based Kalman filtering in solving challenges posed by nonlinear systems.

While modified methods have made some strides in addressing the challenges of parameter identification in non-smooth gap systems, these approaches still face limitations, particularly in accuracy and application [43]. The consequences of inaccurate parameter identification in non-smooth gap systems are significant. Inaccurate models can lead to control strategies that are either too conservative, failing to fully exploit the system's capabilities, or too aggressive, leading to instability or failure. In safety-critical applications, such as aerospace, automotive, or structural engineering, the failure to accurately model and control a nonsmooth system have catastrophic gap consequences.

To address the challenges posed by non-smooth gap systems, advanced filtering algorithms have been developed. Among them, the Strong Tracking Square Root Spherical Simplex-Radial Cubature Quadrature Kalman Filter (STSR-SSRCQKF) stands out for its robustness and accuracy in parameter identification. This method offers several key advantages: 1) This study addresses limitations of the traditional Square Root Unscented Kalman Filter (SR-UKF), which relies on Cholesky decomposition and imposes strict positive-definiteness constraints, risking numerical instability in highly nonlinear or discontinuous systems. By employing QR decomposition for covariance matrix updates, the proposed method removes the dependency on positive definiteness while maintaining high precision. Additionally, the SSRCQKF framework resolves challenges of negative weights in high-dimensional systems by ensuring strictly positive weights and using increased sigma points for improved parameter identification accuracy. 2) The proposed integration of strong tracking factors (STFs) is tailored for state estimation in systems with abrupt geometric nonlinearities. Unlike traditional methods, the STFs is selectively triggered during the first state transition of the system, overcoming the gap value recognition error caused by system discretization and providing more accurate initial values for subsequent Kalman filtering algorithms.



The study is structured as follows: Sect. 2 provides an overview of the state equation of non-smooth gap systems. Section 3 introduces the theory of the proposed STSR-SSRCQKF method in details. Section 4 investigates the performance of the STSR-SSRCQKF algorithm for parameter identification in a simple non-smooth gap system with 1-DoF. Section 5 further validates the effectiveness of this approach in accurately capturing the dynamic behavior of more complex system with 5-DoF, even in the presence of abrupt changes and discontinuities. Through detailed simulations and analysis, the research conclusions are summarized in Sect. 6.

2 State equation of non-smooth gap systems

In a non-smooth gap system, as shown in Fig. 1, the motion of the system is governed by different equations depending on the displacement x of the system relative to predefined thresholds e_1 and e_2 . These thresholds define regions where the system transitions between different states due to the presence of gaps or clearances. The equation can be expressed in Eq. (1). The non-smooth nature of these systems poses challenges for analysis and control, as traditional linear methods may not apply. Understanding and modeling these transitions accurately is crucial for predicting the system's response and ensuring stability and performance in practical applications.

State 2
$$m\ddot{x} + c_1\dot{x} + k_1(x + e_1) = F$$
 when $x < -e_1$
State 1 $m\ddot{x} = F$ when $-e_1 < x < e_2$
State 3 $m\ddot{x} + c_2\dot{x} + k_2(x - e_2) = F$ when $x > e_2$

where m represents the mass of the system. c is the damping coefficient. k represents the stiffness of the

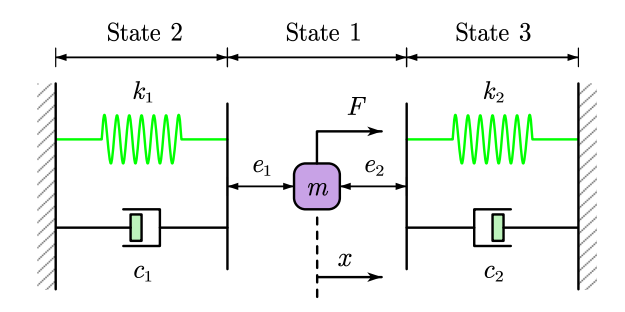


Fig. 1 Schematic diagram of a single degree of freedom system



system. $x \dot{x}$ and \ddot{x} represent the displacement, velocity, and acceleration of the system, respectively. F represents the external force applied to the system. e_1 and e_2 represent the thresholds defining the boundaries between different states.

In State 1, the displacement x is within the gap defined by $-e_1$ and e_1 . The system behaves as if it is in free motion, meaning there is no contact between the components, and thus no restoring force or damping force is acting on the system. The equation simplifies to a basic force balance where the external force F directly influences the acceleration \ddot{x} of the system. This state represents the free travel of the system within the gap.

When the displacement x exceeds the threshold $-e_1$, the system transitions to State 2. The system comes into contact with a boundary or another component, resulting in an additional restoring force and a damping force. The restoring force is proportional to the displacement $(x + e_1)$, reflecting the system's attempt to return to equilibrium. The damping term $c\dot{x}$ accounts for energy dissipation due to the relative motion between the contacting surfaces. This state models the behavior of the system when it is in contact on the left side of the gap.

State 3 is analogous to State 2 but occurs when the displacement x exceeds the threshold e_2 , indicating contact on the right side of the gap. Similar to State 2, the system experiences a restoring force proportional to the displacement $(x - e_2)$ and a damping force $c\dot{x}$. This state captures the system's dynamics when it interacts with the boundary on the right side of the gap.

This set of equations is typically used to model systems where physical constraints or gaps lead to piecewise linear behavior. Examples include mechanical systems with clearances, impact phenomena, and other cases where the system's response changes abruptly depending on the position of its components.

3 STSR-SSRCQKF algorithm

3.1 Standard SSRCQKF algorithm

Consider the following nonlinear dynamic system model, which is characterized by a state equation and a measurement equation:

$$\begin{cases}
X_{k+1} = f(X_k, u_k) + w_k \\
Z_{k+1} = h(X_{k+1}) + v_{k+1}
\end{cases}$$
(2)

In this model, X_{k+1} denotes the state vector of the system at the subsequent time step k + 1. The state vector encapsulates the essential internal variables that describe the system's current condition, which could include variables such as position, velocity, or other quantities pertinent to the specific application. The evolution of the state vector is governed by the nonlinear function f(), which defines the system's dynamics. This function models how the current state X_k , influenced by the system input u_k , transitions to the next state X_{k+1} . Here, u_k represents the sdimensional input vector, which accounts for external controls or forces applied to the system. w_k represents the process noise. Z_{k+1} represents the measurement vector at time stepk + 1. h() represents the measurement function. v_{k+1} represents the measurement noise.

The uncorrelated zero-mean Gaussian white noise processes are as follows:

$$\mathbb{E}(\mathbf{w}_k) = 0, \ \operatorname{cov}(\mathbf{w}_k, \mathbf{w}_i) = \mathbf{Q}_k \mathbf{\delta}_{ki}$$
 (3)

$$\mathbb{E}(\mathbf{v}_k) = 0, \ \operatorname{cov}(\mathbf{v}_{k+1}, \mathbf{v}_i) = \mathbf{R}_k \mathbf{\delta}_{ki} \tag{4}$$

$$cov(\mathbf{w}_k, \mathbf{v}_i) = 0 \tag{5}$$

where, Q_k is the covariance matrix of the process noise, which quantifies the extent of uncertainty present in the system's dynamics at time step k. The Kronecker delta function δ_{kj} indicates that the process

volume rule and arbitrary order Gaussian Laguerre integration rule, respectively, to obtain a new spherical simplex radial volume integration rule. Based on the Bayesian filtering framework, the general and specific forms of SSRCQKF are proposed. This algorithm has 4n+4 (n is the dimension of the state vector) Sigma sampling points, which has higher filtering accuracy (Compared with the traditional UKF algorithm, the UKF algorithm has 2n+1 Sigma points), but also means that the calculation is more time-consuming. The standard SSRCQKF algorithm is as follows:

(1) Initialization.

The process begins with the initialization of the state estimate and covariance matrix. The initial estimate of the state vector is the expected value of the state. The covariance matrix represents the uncertainty in the initial state estimate. The initialization step provides the baseline from which all subsequent updates are performed.

$$\hat{X}_0 = \mathbf{E}[X_0] \tag{6}$$

$$\boldsymbol{P}_0 = \mathrm{E}\left[\left(\boldsymbol{X}_0 - \hat{\boldsymbol{X}}_0 \right) \left(\boldsymbol{X}_0 - \hat{\boldsymbol{X}}_0 \right)^{\mathrm{T}} \right] \tag{7}$$

where $\hat{X_0}$ represents the initial value of the state vector, P_0 is the initial error covariance matrix, and the superscript T represents the transpose of the matrix.

(2) Sigma points generation.

In SSRCQKF, the sigma points $(\chi_{k|k}^i)$ are generated as shown in Eq. (8).

$$\chi_{k|k}^{i} = \begin{cases}
\hat{X}_{k|k} + \sqrt{(n+2+\sqrt{2n+4})P_{k}}[\mathbf{a}, -\mathbf{a}]_{i}, i = 1, 2, \dots, 2n+2 \\
\hat{X}_{k|k} + \sqrt{(n+2-\sqrt{2n+4})P_{k}}[\mathbf{a}, -\mathbf{a}]_{i-2n-2}, i = 2n+3, \dots, 4n+4
\end{cases} (8)$$

noise is uncorrelated over time, meaning that the noise at any time step k is independent of the noise at any other time step j. \mathbf{R}_k represents the covariance matrix of the measurement noise, which captures the level of uncertainty in the system's observations at time step k.

Spherical simplex-radial cubature quadrature Kalman filter (SSRCQKF) algorithm decomposes the Gaussian probability weighted integral of nonlinear functions into spherical integral and radial integral, and approximates them using spherical simplex

where the subscript i in $[a, -a]_i$ represents the i-th column of the matrix. The elements $a_{i,j}$ in the matrix a are calculated as shown in Eq. (9), and in the formula, $i = 1, 2, \dots, n+1$.

$$a_{i,j} = \begin{cases} -\sqrt{\frac{n+1}{n(n-j+2)(n-j+1)}}, & j < i \\ 0, & j > i \\ \sqrt{\frac{(n+1)(n-i+1)}{n(n-i+2)}}, & i = j \end{cases}$$



(3) Time update.

The sigma points generated in the previous step are propagated through the system's nonlinear dynamics to predict the state at the next step. Equation (10) represents the propagation of each sigma point through the system dynamics f(). In Eq. (11), the predicted state $\widehat{X}_{k+1|k}$ is computed as a weighted sum of the propagated sigma points. Equation (12) updates the covariance based on the propagated sigma points and includes the process noise Q_k .

$$\hat{X}_{k+1|k}^{i} = f(\chi_{k|k}^{i})$$
 $(i = 1, \dots, 4n + 4)$ (10)

$$\hat{X}_{k+1|k} = \frac{n}{4(n+1)(n+2+\sqrt{2n+4})} \sum_{i=1}^{2n+2} \hat{X}_{k+1|k}^{i} + \frac{n}{4(n+1)(n+2-\sqrt{2n+4})} \sum_{i=2n+3}^{4n+4} \hat{X}_{k+1|k}^{i}$$
(11)

$$\begin{aligned} & \boldsymbol{P}_{k+1|k} = \frac{n}{4(n+1)(n+2+\sqrt{2n+4})} \\ & \sum_{i=1}^{2n+2} \left(\hat{\boldsymbol{X}}_{k+1|k}^{i} - \hat{\boldsymbol{X}}_{k+1|k} \right) \left(\hat{\boldsymbol{X}}_{k+1|k}^{i} - \hat{\boldsymbol{X}}_{k+1|k} \right)^{\mathrm{T}} \\ & + \frac{n}{4(n+1)(n+2-\sqrt{2n+4})} \\ & \sum_{i=2n+3}^{4n+4} \left(\hat{\boldsymbol{X}}_{k+1|k}^{i} - \hat{\boldsymbol{X}}_{k+1|k} \right) \left(\hat{\boldsymbol{X}}_{k+1|k}^{i} - \hat{\boldsymbol{X}}_{k+1|k} \right)^{\mathrm{T}} + \boldsymbol{Q}_{k} \end{aligned}$$

$$(12)$$

where $P_{k+1|k}$ refers to the state prediction error covariance matrix from time step k to k+1. The subscript k+1|k explicitly indicates the time progression from k to k+1. indicates the specific time step.

(4) New sigma points generation.

Following the time update, a new set of sigma points is generated based on the updated state estimate and covariance matrix:

(5) Measurement prediction.

The sigma points are transformed through the model to predict the measurement. Each sigma point is passed through the measurement function h() to generate predicted measurements. The predicted measurement $\widehat{Z}_{k+1|k}$ is computed as a weighted sum of the predicted sigma points with Eq. (15). Equation (16) updates the measurement covariance matrix $P_{zz,k+1}$. The cross covariance $P_{xz,k+1}$ between the state and measureme $\widehat{Z}_{k+1|k}^i = h\left(\chi_{k+1|k}^i\right)$ nt is computed based on the spread of the predicted measurement sigma points, as shown in Eq. (17).

$$\hat{\mathbf{Z}}_{k+1K}^{i} = h(\mathbf{\chi}_{k+1k}^{i}) \tag{14}$$

$$\hat{\mathbf{Z}}_{k+1|k} = \frac{n}{4(n+1)(n+2+\sqrt{2n+4})} \sum_{i=1}^{2n+2} \hat{\mathbf{Z}}_{k+1|k}^{i} + \frac{n}{4(n+1)(n+2-\sqrt{2n+4})} \sum_{i=2n+3}^{4n+4} \hat{\mathbf{Z}}_{k+1|k}^{i}$$
(15)

$$P_{zz,k+1} = \frac{n}{4(n+1)(n+2+\sqrt{2n+4})}$$

$$\sum_{i=1}^{2n+2} (\hat{\mathbf{Z}}_{k+1|k}^{i} - \hat{\mathbf{Z}}_{k+1|k}) (\hat{\mathbf{Z}}_{k+1|k}^{i} - \hat{\mathbf{Z}}_{k+1|k})^{\mathrm{T}}$$

$$+ \frac{n}{4(n+1)(n+2-\sqrt{2n+4})}$$

$$\sum_{i=2n+3}^{4n+4} (\hat{\mathbf{Z}}_{k+1|k}^{i} - \hat{\mathbf{Z}}_{k+1|k}) (\hat{\mathbf{Z}}_{k+1|k}^{i} - \hat{\mathbf{Z}}_{k+1|k})^{\mathrm{T}} + \mathbf{R}_{k+1}$$
(16)

$$\chi_{k+1|k}^{i} = \begin{cases} \hat{X}_{k+1|k} + \sqrt{(n+2+\sqrt{2n+4})} P_{k+1|k} [a, -a]_{i}, i = 1, 2, \dots, 2n+2\\ \hat{X}_{k+1|k} + \sqrt{(n+2-\sqrt{2n+4})} P_{k+1|k} [a, -a]_{i-2n-2}, i = 2n+3, \dots, 4n+4 \end{cases}$$
(13)



$$P_{xz,k+1} = \frac{n}{4(n+1)(n+2+\sqrt{2n+4})}$$

$$\sum_{i=1}^{2n+2} (\hat{X}_{k+1|k}^{i} - \hat{X}_{k+1|k}) (\hat{Z}_{k+1|k}^{i} - \hat{Z}_{k+1|k})^{\mathrm{T}}$$

$$+ \frac{n}{4(n+1)(n+2-\sqrt{2n+4})}$$

$$\sum_{i=2n+3}^{4n+4} (\hat{X}_{k+1|k}^{i} - \hat{X}_{k+1|k}) (\hat{Z}_{k+1|k}^{i} - \hat{Z}_{k+1|k})^{\mathrm{T}}$$
(17)

where, $P_{zz,k+1}$ represents the output prediction self-covariance matrix at time step k+1. Here, the subscript zz specifies that it is a self-covariance matrix, while k+1 indicates the specific time step. $P_{xz,k+1}$ denotes the output prediction cross-covariance matrix at time step k+1. Here, the subscript xz highlights that it is a cross-covariance matrix, and k+1 again marks the corresponding time step.

(6) Measurement update.

Finally, the filter updates the state estimate and covariance based on the new measurement. The Kalman gain $K_{g,k+1}$ determines the weight given to the measurement residual $(\mathbf{Z}_{k+1} - \widehat{\mathbf{Z}}_{k+1|k})$ in updating the state estimate. The state estimate is updated using the Kalman gain and the difference between the actual and predicted measurements with Eq. (19). The covariance matrix $P_{k+1|k+1}$ is similarly updated to reflect the reduction in uncertainty following the incorporation of the new measurement, as shown in Eq. (20).

$$\mathbf{K}_{g,k+1} = \mathbf{P}_{xz,k+1} \mathbf{P}_{zz,k+1}^{-1} \tag{18}$$

$$\hat{X}_{k+1} = \hat{X}_{k+1|k} + K_{g,k+1} \left(\mathbf{Z}_{k+1} - \hat{\mathbf{Z}}_{k+1|k} \right)$$
 (19)

$$\mathbf{P}_{k+1|k+1} = \mathbf{P}_{k+1|k} - \mathbf{K}_{g,k+1} \mathbf{P}_{zz,k+1} \mathbf{K}_{g,k+1}^{\mathrm{T}}$$
 (20)

The SSRCQKF process iterates through these steps, updating the state and covariance estimates at each time step based on the system dynamics and measurements.

3.2 Improved SR-SSRCQF algorithm

The Improved Square Root Spherical simplex-radial cubature quadrature Kalman filter (SR-SSRCQKF) algorithm addresses a critical issue encountered in the traditional Cholesky decomposition method used for calculating the square root of the error covariance

matrix, as shown in Eqs. (8) and (13) with the recursive process. Specifically, the Cholesky decomposition requires the covariance matrix to be positive definite. However, due to the influence of computer rounding errors during numerical computations, the positive definiteness of the covariance matrix may not always be guaranteed. To overcome this limitation, the SR-SSRCQF algorithm leverages QR decomposition, providing a more robust solution for computing the square root of the matrix.

(1) QR decomposition-based covariance matrix calculation.

In the SR-SSRCQF algorithm, the error covariance matrix at the prediction step, denoted as $P_{k+1|k}$, can be expressed as:

$$P_{k+1|k} = S_{k+1|k} S_{k+1|k}^{\mathrm{T}}$$
(21)

where, $S_{k+1|k}$ represents the square root of the covariance matrix. To compute this square root, QR decomposition is applied.

By expressing $S_{k+1|k}^{T}$ as the product of an orthogonal matrix q and an upper triangular matrix r:

$$S_{k+1|k}^{\mathrm{T}} = q\mathbf{r} \tag{22}$$

The square root of the covariance matrix can be redefined in Eq. (23). This alternative expression ensures that the square root of the covariance matrix is computed more reliably, even in cases where the traditional Cholesky decomposition may fail due to numerical inaccuracies.

$$S_{k+1|k} = \mathbf{r}^{\mathrm{T}} \tag{23}$$

(2) Derivation of the covariance matrix square root. From the QR decomposition, the following expression for the square root of the covariance matrix is derived:

$$\mathbf{r}_{1} = \operatorname{qr} \begin{pmatrix} \left[\sqrt{\omega^{c_{1}}} \left(\hat{\mathbf{X}}_{k+1|k}^{1:2n+2} - \hat{\mathbf{X}}_{k+1|k} \right) \left(\hat{\mathbf{X}}_{k+1|k}^{1:2n+2} - \hat{\mathbf{X}}_{k+1|k} \right)^{\mathrm{T}}, \\ \sqrt{\omega^{c_{2}}} \left(\hat{\mathbf{X}}_{k+1|k}^{2n+3:4n+4} - \hat{\mathbf{X}}_{k+1|k} \right) \left(\hat{\mathbf{X}}_{k+1|k}^{2n+3:4n+4} - \hat{\mathbf{X}}_{k+1|k} \right)^{\mathrm{T}}, \\ \sqrt{\mathbf{Q}_{k}} \right]^{\mathrm{T}} \end{pmatrix}$$

$$(24)$$

where, qr() represents QR decomposition,
$$\omega^{c_1} = \frac{n}{4(n+1)(n+2+\sqrt{2n+4})}$$
, $\omega^{c_2} = \frac{n}{4(n+1)(n+2-\sqrt{2n+4})}$.

The new form of the square root of the covariance matrix is then given in Eq. (25). This formulation allows the covariance matrix to be computed



accurately, even in the presence of potential numerical instabilities.

$$S_{k+1|k} = \mathbf{r}_1^{\mathrm{T}} \tag{25}$$

(3) Measurement update and Kalman gain.

The Kalman gain $K_{g,k+1}$ can be updated using the square root forms of the covariance matrices. Specifically, the Kalman gain is computed as:

$$\mathbf{K}_{g,k+1} = \mathbf{P}_{xz,k+1} / \left(\mathbf{S}_{zz,k+1} \mathbf{S}_{zz,k+1}^{\mathrm{T}} \right)$$
 (26)

where $S_{zz,k+1}$ represents the square root of the measurement covariance matrix.

According to the definition of covariance of state estimation error:

$$\begin{aligned}
\mathbf{P}_{k+1|k+1} &= \operatorname{cov}(\mathbf{X}_{k+1} - \hat{\mathbf{X}}_{k+1|k+1}) \\
&= \operatorname{cov}(\mathbf{X}_{k+1}) \\
&- (\hat{\mathbf{X}}_{k+1|k} + \mathbf{K}_{k+1} (\mathbf{Z}_{k+1} - \mathbf{Z}_{k+1|k})))
\end{aligned} (27)$$

This simplifies to:

$$P_{k+1|k+1} = \text{cov}((I - K_{g,k+1}H_{k+1})(X_{k+1} - \widehat{X}_{k+1|k})) + \text{cov}(K_{k+1}V_{k+1})$$

$$= (I - K_{k+1}H_{k+1})\text{cov}(X_{k+1} - \widehat{X}_{k+1|k})(I - K_{g,k+1}H_{k+1})^{\text{T}} + K_{k+1}\text{cov}(V_{k+1})K_{k+1}^{\text{T}}$$

$$= (I - K_{g,k+1}H_{k+1})P_{k+1|k}(I - K_{g,k+1}H_{k+1})^{\text{T}} + K_{g,k+1}R_{k+1}K_{g,k+1}^{\text{T}}$$

$$= (I - K_{g,k+1}H_{k+1})S_{k+1|k}S_{k+1|k}^{\text{T}}(I - K_{g,k+1}H_{k+1})^{\text{T}} + K_{g,k+1}\sqrt{R_{k+1}}\sqrt{R_{k+1}}\sqrt{R_{k+1}}^{\text{T}}K_{g,k+1}^{\text{T}}$$

$$+ K_{g,k+1}\sqrt{R_{k+1}}\sqrt{R_{k+1}}^{\text{T}}K_{g,k+1}^{\text{T}}$$
(28)

where H_{k+1} is the Jacobian matrix of the measurement function at time k + 1, I is the unit matrix.

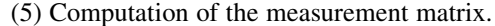
(4) Final covariance matrix square root update.

The final step involves applying QR decomposition to update the square root of the covariance matrix:

$$\mathbf{r}_{2} = \operatorname{qr}\left(\left[\left(\mathbf{I} - \mathbf{K}_{g,k+1}\mathbf{H}_{k+1}\right)\mathbf{S}_{k+1|k}, \mathbf{K}_{g,k+1}\sqrt{\mathbf{R}_{k+1}}\right]^{\mathrm{T}}\right)$$
(29)

The square root of the updated covariance matrix is then obtained as:

$$S_{k+1|k+1} = \mathbf{r}_2^{\mathrm{T}} \tag{30}$$



For complex nonlinear structures, if there is a nonlinear relationship between the observation vector and the state vector, the equivalent form of the measurement matrix can be used to avoid calculating the Jacobian matrix.

According to the definition, the state prediction self covariance matrix $P_{k+1|k}$, the output prediction self covariance matrix $P_{zz,k+1}$, and the output prediction cross covariance matrix $P_{xz,k+1}$ can be written in the form of Eqs. (31),(32) and (33).

$$\mathbf{P}_{k+1|k} = \mathrm{E}[(\mathbf{X}_{k+1} - \hat{\mathbf{X}}_{k+1|k})(\mathbf{X}_{k+1} - \hat{\mathbf{X}}_{k+1|k})^{\mathrm{T}}]$$
 (31)

$$P_{zz,k+1} = E[(\mathbf{Z}_{k+1} - \hat{\mathbf{Z}}_{k+1|k})(\mathbf{Z}_{k+1} - \hat{\mathbf{Z}}_{k+1|k})^{T}]$$

$$= \mathbf{H}_{g,k+1}E[(\mathbf{X}_{k+1} - \hat{\mathbf{X}}_{k+1|k})(\mathbf{X}_{k+1} - \hat{\mathbf{X}}_{k+1|k})^{T}]$$

$$\mathbf{H}_{g,k+1}^{T} = \mathbf{H}_{g,k+1}\mathbf{P}_{k+1|k}\mathbf{H}_{g,k+1}^{T}$$
(32)

$$\mathbf{P}_{xz,k+1} = \mathrm{E}[(\mathbf{X}_{k+1} - \hat{\mathbf{X}}_{k+1|k}) (\mathbf{Z}_{k+1} - \hat{\mathbf{Z}}_{k+1|k})^{\mathrm{T}}]
= \mathrm{E}[(\mathbf{X}_{k+1} - \hat{\mathbf{X}}_{k+1|k}) (\mathbf{X}_{k+1} - \hat{\mathbf{X}}_{k+1|k})^{\mathrm{T}}] \mathbf{H}_{g,k+1}
= \mathbf{P}_{k+1|k} \mathbf{H}_{g,k+1}^{\mathrm{T}}$$
(33)

The equivalent form of the measurement matrix can be obtained as:

$$\mathbf{H}_{k+1} = [(\mathbf{P}_{k+1|k})^{-1} \mathbf{P}_{xz,k+1}]^{\mathrm{T}} = (\mathbf{P}_{xz,k+1})^{\mathrm{T}} (\mathbf{P}_{k+1|k})^{-1}
= (\mathbf{P}_{xz,k+1})^{\mathrm{T}} (\mathbf{S}_{k+1|k} \mathbf{S}_{k+1|k}^{\mathrm{T}})^{-1}$$
(34)

The improved SR-SSRCQF algorithm, by employing QR decomposition instead of Cholesky decomposition, provides a more stable and reliable method for updating the square root of the covariance matrix. This approach mitigates the issues arising from numerical errors, ensuring the positive definiteness of the covariance matrix and enhancing the overall performance of the filter in nonlinear state estimation problems.

3.3 Strong tracking factor

In the context of parameter identification and state estimation for intermittent systems, one of the primary challenges is accurately determining the system's operating state, particularly when the system



undergoes state transitions. Intermittent systems are characterized by abrupt shifts between distinct states, which can cause significant discrepancies between observed and predicted quantities if the state prediction equations are not promptly adjusted. This issue is particularly pronounced during the first transition from one state to another, such as from State 1 to State 2 or State 3. To address this challenge, a strong tracking factor is introduced, which helps to identify state transitions by leveraging the sudden changes in residual information.

The strong tracking factor, denoted as μ_{k+1} , is a key element in detecting state transitions in intermittent systems. This factor is designed to adaptively adjust the filtering process in response to changes in the system's state, ensuring that the filter remains accurate even when the system transitions between different operating modes. The strong tracking factor is particularly useful during the first entry into a new state, where the discrepancy between predicted and observed quantities is likely to be most pronounced.

The strong tracking factor μ_{k+1} is computed using the following equations:

$$\mu_{k+1} = \begin{cases} \mu_k & \mu_{k+1} \ge 1\\ 1 & \mu_{k+1} < 1 \end{cases}$$
 (35)

$$\mu_{k+1} = \frac{\text{tr}[N_{k+1}]}{\text{tr}[M_{k+1}]} \tag{36}$$

$$N_{k+1} = \Gamma_{k+1} - H_{k+1} Q_{k+1} H_{k+1}^{\mathrm{T}} - l R_{k+1}$$
 (37)

$$\mathbf{M}_{k+1} = \mathbf{H}_{k+1} \mathbf{\Phi}_{k+1|k} \mathbf{P}_{k+1|k} \mathbf{\Phi}_{k+1|k}^{\mathrm{T}}
= \mathbf{H}_{k+1} [\mathbf{P}_{k+1|k} - \mathbf{Q}_{k+1}] \mathbf{H}_{k+1}^{\mathrm{T}}
= \mathbf{H}_{k+1} [\mathbf{S}_{k+1|k} \mathbf{S}_{k+1|k}^{\mathrm{T}} - \mathbf{Q}_{k+1}] \mathbf{H}_{k+1}^{\mathrm{T}}$$
(38)

where, $\operatorname{tr}[]$ denotes the trace of a matrix, which is the sum of the diagonal elements and provides a scalar representation of the matrix's characteristics, $l \geq 1$, is a weakening factor, and $\Phi_{k+1|k}$ is the state transition matrix, which only appears as a process variable and is not included in the final result.

The output residual sequence ε_k , defined as the difference between the observed measurement \mathbf{Z}_k and the predicted measurement $\hat{\mathbf{Z}}_k$, is a crucial component in determining the strong tracking factor:

$$\mathbf{\varepsilon}_k = \mathbf{Z}_k - \hat{\mathbf{Z}}_k \tag{39}$$

The actual output residual sequence Γ_{k+1} is calculated as follows:

$$\Gamma_{k+1} = \begin{cases}
\mathbf{\varepsilon}_1 \mathbf{\varepsilon}_1^T & k = 1 \\
\rho \Gamma_k + \mathbf{\varepsilon}_{k+1} \mathbf{\varepsilon}_{k+1}^T & k \ge 2
\end{cases}$$
(40)

where, $0 < \rho \le 1$ is a weighting factor that controls the influence of past residuals on the current estimate. This study adopts $\rho = 0.95$ to ensure consistency and comparability with previous works [44, 45]. The sequence Γ_{k+1} represents the accumulated residual information, which is used to adjust the filter's sensitivity to state changes.

The strong tracking factor μ_{k+1} is essential for maintaining the accuracy of state estimation in intermittent systems. For example, when the system transitions from state 1 to state 2, there is a significant difference between the observed values estimated by the physical model of state 1 and the actual observed values. At this time, the calculated strong tracking factor will also have a large amplitude jump. Then, based on the given velocity sign, current displacement state, and other conditions, it is determined whether a state transition is necessary. Therefore, by dynamically adjusting the filtering process based on residual information, the strong tracking factor enables the system to quickly and accurately detect state transitions, minimizing errors between predicted and observed quantities. This is particularly important in systems where state transitions are infrequent but have a significant impact on system behavior.

3.4 Overall system identification flowchart

The flowchart presented in Fig. 2 illustrates the algorithmic procedure of the STSR-SSRCQKF used for state estimation in non-smooth gap systems. The process begins with initialization, where the initial state, covariance matrices, and system parameters are established. Following this, the algorithm enters the status judgment phase, where it assesses the current state of the system to determine the need for further updates.

Subsequently, the algorithm proceeds to the generation of sigma points, a critical step in the unscented transform process, which is carried out twice-once after a predetermined time update and again after a measurement update. The sigma points are used to



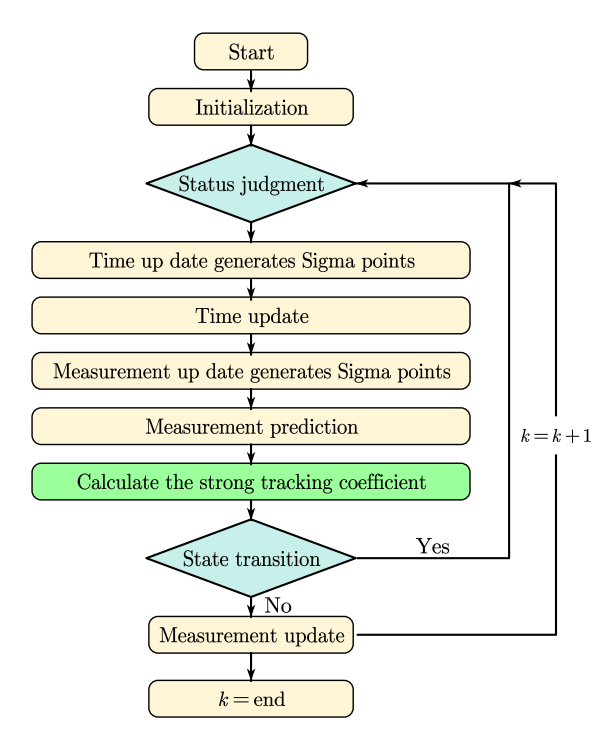


Fig. 2 Process diagram for gap system state estimation and parameter identification

predict the system's measurements based on the current state estimates.

The core of the algorithm is the calculation of the strong tracking coefficient, highlighted in green, which ensures the filter's robustness to sudden changes in the system dynamics. This coefficient dynamically adjusts the Kalman gain, allowing the filter to "strongly track" the true state of the system, particularly in the presence of non-smooth transitions.

It is important to note that the strong tracking factor proposed in this study is triggered only under specific conditions. When the strong tracking factor exceeds the predefined threshold and the initial gap value on one side is still zero, the displacement at that moment is taken as the first identified gap value on that side. Subsequently, the system transitions into a new state, where the SR-SSRCQKF algorithm is used for precise gap identification. Future state transitions are determined based on the previously identified gap value. The reasoning behind this approach is as follows:

 When the system transitions from state 1 to other states for the first time, there is a significant change in the strong tracking factor, making this state jump easier to capture. The

- displacement at that moment closely approximates the true gap value, but due to the system's discrete sampling, it is unlikely to exactly match the actual gap value.
- The SR-SSRCQKF algorithm can more accurately identify the gap value, making it a more reliable criterion for determining state transitions during subsequent recursive processes.
- 3) The strong tracking factor is triggered only once on each side of the system, improving the stability of the recursive process and preventing the system from repeatedly jumping at the gap edge due to noise interference.

After the state transition, where the system evolves according to its underlying dynamic model, the measurement update phase follows. Here, the predicted measurements are compared against the actual sensor readings, and the state estimates are updated accordingly. This process is iterative, with the index k incrementing until the algorithm reaches the predefined end condition.

The proposed method is particularly well-suited for real-time implementation due to its practical use of acceleration data as input. Unlike traditional approaches that often require velocity or displacement measurements—data that can be more challenging to obtain or less reliable in dynamic environments—this method focuses on acceleration data, which is more readily available and typically less prone to noise in many engineering applications.

4 Simulation of single-degree-of-freedom nonsmooth gap systems

4.1 DoF non-smooth gap System descriptions

The proposed method's effectiveness is firstly validated using a one-dimensional nonlinear system, as depicted in Fig. 1. The system's actual parameters are defined as follows: mass m = 1kg, damping coefficients $c_1 = 1$ N·s/m and $c_2 = 1$ N·s/m, stiffness constants $k_1 = 100$ N/m and $k_2 = 150$ N/m. The external load applied to the system is a sine wave given by $F(t) = -\sin(0.1\pi t)$, with a sampling frequency of 500 Hz. The fourth-order Runge Kutta method is used to discretize the transition and measurement



equations, and assuming the input is known, the observed value is acceleration.

The system is composed of three distinct states. State 1 occurs when the mass is positioned between two gaps, where the state vector includes only two variables: displacement and velocity. When the mass crosses the left gap, the system transitions into State 2, and the augmented state vector then includes displacement, velocity, stiffness k_1 , damping coefficient c_1 , and gap value e_1 ; Similarly, when the mass crosses the right gap, the system enters State 3, and the augmented state vector comprises displacement, velocity, stiffness k_2 , damping coefficient c_2 , and gap value.

The initial conditions for the three state vectors are defined as follows: $X_{\text{State1},t=0} = [x, \dot{x}] = [0, 0],$ $X_{\text{State2},t=0} = [x, \dot{x}, k_1, c_1, e_1] = [0, 0, 70, 0.7, 0],$ $X_{\text{State3},t=0} = [x, \dot{x}, k_2, c_2, e_2] = [0, 0, 105, 0.7, 0]e_2.$

The initial state error covariance matrices are specified as follows: $P_{\text{State1},t=0} = \text{diag}\left[\sigma_x^2, \sigma_x^2\right] = \text{diag}[1 \times 10^{-1}, 1 \times 10^{-2}], \qquad P_{\text{State2},t=0} = \text{diag}\left[\sigma_x^2, \sigma_x^2\right] = \text{diag}\left[\sigma_x^2, \sigma_{c_1}^2, \sigma_{$

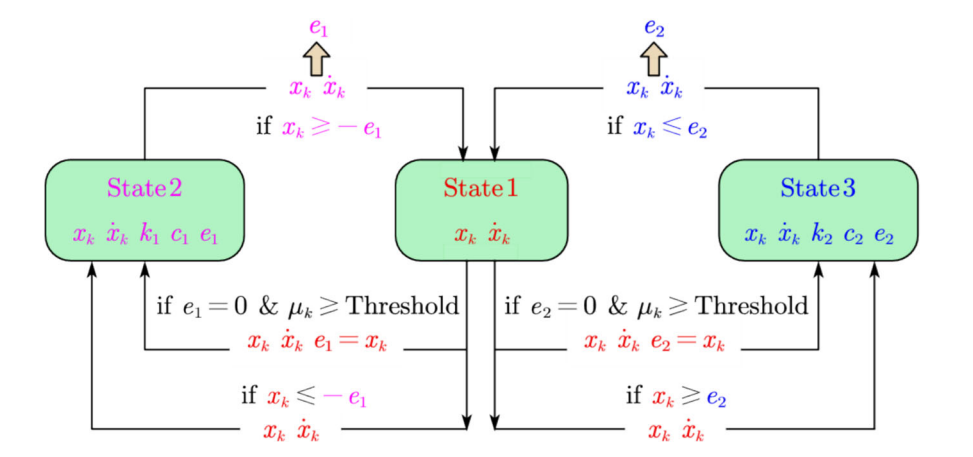
Additionally, the covariance matrices for the initial system process noise are defined as: $\mathbf{Q}_{\text{State1},t=0}$ = diag $[\sigma_x^2, \sigma_x^2]$ = diag $[1 \times 10^{-10}, 1 \times 10^{-10}]$, $\mathbf{Q}_{\text{State2},t=0}$ = diag $[\sigma_x^2, \sigma_x^2, \sigma_{k_1}^2, \sigma_{c_1}^2, \sigma_{e_1}^2,]$ = diag $[1 \times 10^{-10}, 1 \times 10^{-10}, 1 \times 10^{-8}, 1 \times 10^{-8}, 1 \times 10^{-10}]$, $\mathbf{Q}_{\text{State3},t=0}$ = diag $[\sigma_x^2, \sigma_x^2, \sigma_{k_2}^2, \sigma_{c_2}^2, \sigma_{e_2}^2,]$ = diag $[1 \times 10^{-10}, 1 \times 10^{-10}]$, $[1 \times 10^{-10}, 1 \times$

Fig. 3 Schematic diagram of 1-DoF state transition and variable transfer

 10^{-10} , 1×10^{-10} , 1×10^{-8} , 1×10^{-8} , 1×10^{-10}]. In this manuscript, the covariance matrix of process noise and observation noise is initialized based on experience. The main summary of this experience is that the more accurate the physical model, the smaller the covariance matrix Q of process noise, and its specific value is also related to the corresponding parameter order. For example, for physical quantities such as displacement and velocity that describe the system's motion state, the usual value is $10^{-2} \sim 10^{-4}$, and for the parameters to be identified, the usual value is $10^{-8} \sim 10^{-12}$. For the covariance matrix R of observation noise, when the error of the observation is large, the value of R increases accordingly, and its value is usually between 10^0 and 10^{-3} .

Figure 4 represents different aspects of the system's response and state transitions in a 1-DoF non-smooth gap system. Figure 4 a shows the displacement response of the system over time across the three different states (State 1, State 2, and State 3), while Fig. 4 b compares the estimated total displacement against the real total displacement within the three states.

Figure 3 illustrates the state transition and parameter identification process in a non-smooth gap system. When conducting parameter identification and state estimation, the strong tracking factor is calculated from the second time step onward. If this factor exceeds a predefined threshold for the first time and the velocity of the mass block is negative, the system transitions from State 1 to State 2. During this transition, the displacement and velocity values from State 1 at the current time step are transferred to State 2, and the gap value in State 2 is updated to $e_1 = x_k$. At





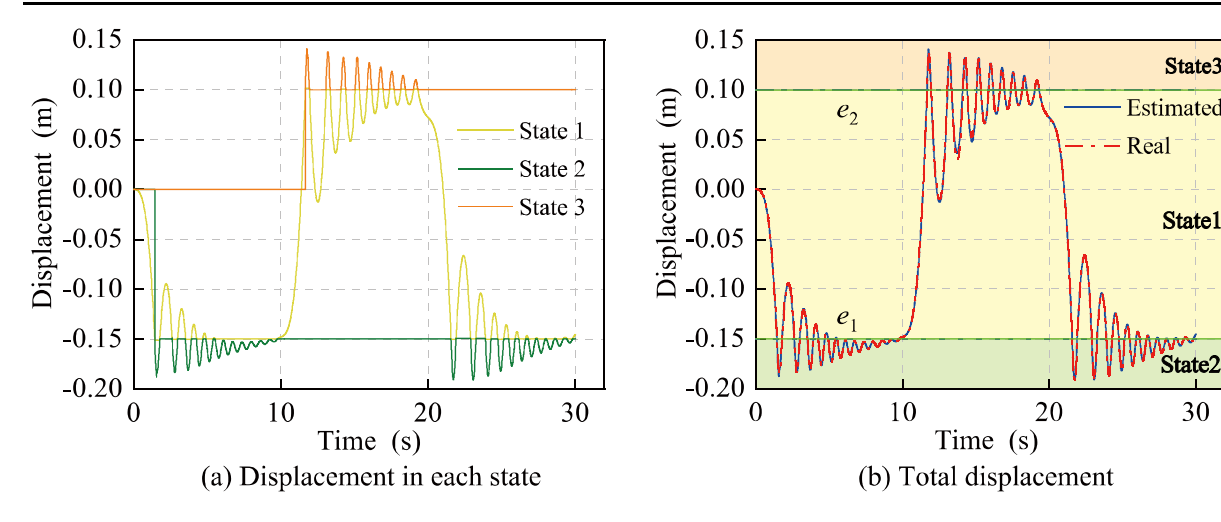


Fig. 4 Displacement responses in the 1-DoF non-smooth gap system

this point, the strong tracking factor on the left becomes ineffective. In future operations, the transition from State 1 to State 2 depends on the gap value e_1 identified in State 2. Subsequent transitions between State 1 and State 2 involve only the displacement and velocity values, without transferring the gap value e_1 . In this example, the threshold for the strong tracking factor is set to 10. The transition process and parameter transfer between State 1 and State 3 follow the same logic.

4.2 Performance of the proposed method

The displacement responses of the system under the specified sine-wave load are illustrated in Fig. 4. The system starts in State 1, where the mass is moving within the range without crossing any gaps. The displacement is relatively low, as shown in Fig. 4 a. When the mass crosses the left gap, the system transitions into State 2, leading to a sharp increase in displacement. This state is marked by higher displacement values. As the system continues, it crosses the right gap, transitioning into State 3. The displacement again changes and the behavior reflects the dynamics within this new state. Figure 4 b shows a close match between the estimated and real displacements, indicating the effectiveness of the proposed method in accurately estimating the displacement throughout the transitions, particularly in handling non-linearities and abrupt changes in the system's behavior.

Figure 5 illustrate the parameter identification results, and each subplot compares the estimated

parameter values (blue line) with their true values (red dashed line) over time. When the system transits from State 1 to State 2 and State 3, the method accurately and rapidly identifies the stiffness and gaps in these states $(k_1, k_2, e_1, \text{ and } e_2)$. Damping ratios could be accurately identified in the later moments. The close alignment between the estimated and true values across different parameters confirms the reliability of the proposed STSR-SSRCQKF method.

As shown in Fig. 5 a and Fig. 5 d, the system transitions from state 2 to state 1 at 1.432 s, allowing stiffness parameter k_1 to be identified first. At 11.672 s, the system transitions from state 2 to state 3, and only then does the identification of stiffness parameter k_2 begin, with its value rapidly converging to the true value. Figure 5 b illustrates that the damping parameter c_1 experiences significant fluctuations during the state transition. Once the system transitions back from state 2 to state 1, c_1 is no longer identified, and its value remains constant until the final seconds, when the system re-enters state 2, and c_1 gradually converges to its true value. Figure 5 c and Fig. 5 f demonstrate that the strong tracking factor proposed in this paper can accurately detect the system's first state transition, with the initial gap value being very close to the true value. The SR-SSRCQKF algorithm further refines this to obtain an accurate gap value.

Furthermore, Fig. 6 depicts the matching of state transitions with strong tracking factors. Figure 6 b shows that the strong tracking factors spike at specific times, corresponding to the moments when the system



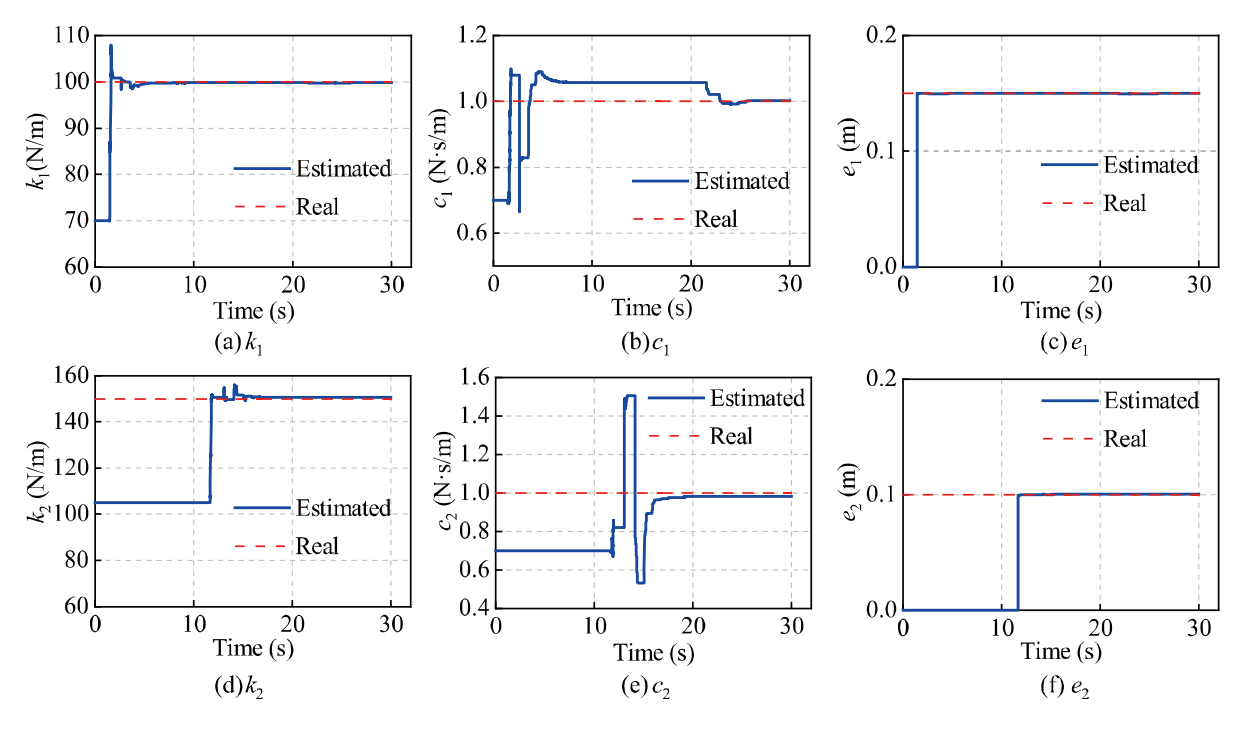
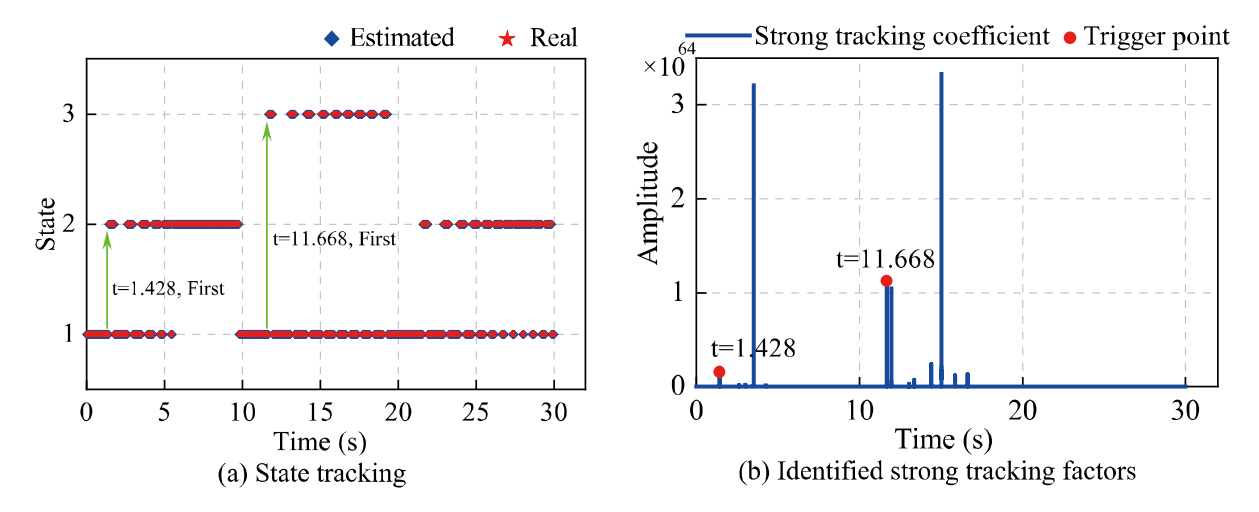


Fig. 5 Parameter identification results of the 1-DoF non-smooth gap system



 $\textbf{Fig. 6} \quad \text{Matching of state transitions and strong tracking factors in the 1-DoF non-smooth gap system}$

transitions between states (as depicted in Fig. 6 a). These spikes ensure that the method quickly adjusts to the new state, maintaining accurate tracking despite the non-smooth nature of the transitions. The synchronization between state tracking and strong tracking factors underscores the method's ability to adapt to sudden changes in the system, ensuring continuous and accurate state estimation.

In Fig. 6 b, multiple peaks appear. As previously mentioned, the strong tracking factor is triggered only under specific conditions, enabling the system's first state transition either to the left or right. This approach not only ensures the algorithm's identification accuracy but also improves its stability when recognizing the gap system. As a result, the strong tracking factor is only activated twice, as indicated at t = 1.428s and



t = 11.668s. The other peaks in the figure also correspond to system state transitions, but if the system tracks the states well, these peaks may not exceed the set threshold. During the first state transition, however, the strong tracking factor shows a significant change.

To simulate the interference of noise in actual observations and verify the robustness of the proposed method, white Gaussian noise was added to the measurements. The performance of the parameter identification approach under varying noise levels is summarized in Table 1. The table provides a comparison between the true, initial, and estimated values of the parameters $k_1, k_2, c_1, c_2, e_1, e_2$ under noise free and 3% RMS(root mean square) white Gaussian noise conditions. The results show that the proposed method accurately identifies the system parameters with minimal error, particularly when dealing with real-world conditions characterized by noise and abrupt transitions between states.

5 Computational simulations of a 5-DoF dual gap system

5.1 5-DoF dual gap system descriptions

To further validate the effectiveness of the proposed method, a 5-DoF dual gap system was used for verification. This complex system is shown in Fig. 7. The system also includes three states, and its dynamic equation is shown in Eq. (41).

Table 1 Parameter identifications under different noise levels in the 1-DoF non-smooth gap system

Parameter	True value	Initial value	Noise free		3% noise	
			Estimated value	Error (%)	Estimated value	Error (%)
k_1	100	$0.7 k_1$	100.0	0.0	100.0	0.0
k_2	150	$0.7 \ k_2$	150.7	0.5	150.7	0.5
c_1	1.0	$0.7 c_1$	0.99856	- 0.1	0.99856	- 0.1
c_2	1.0	$0.7 \ c_2$	0.98801	- 1.2	0.98801	- 1.2
e_1	0.15	0	0.1497	- 0.2	0.1497	- 0.2
e_2	0.10	0	0.1001	0.1	0.1001	0.1

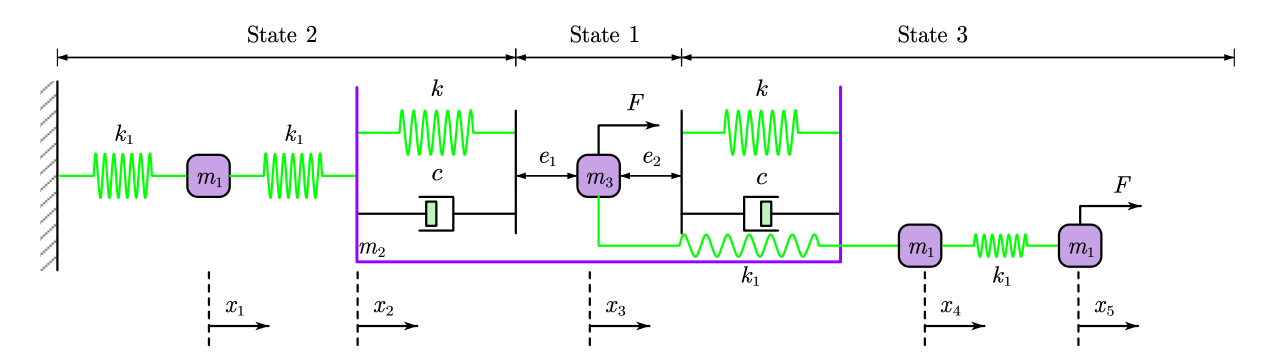


Fig. 7 Non-smooth gap system with 5-DoF



$$M_{s1} = \begin{bmatrix} m_1 & 0 \\ 0 & m_2 \end{bmatrix}$$
 $M_{s2} = \begin{bmatrix} m_3 & 0 & 0 \\ 0 & m_1 & 0 \\ 0 & 0 & m_1 \end{bmatrix}$

$$\mathbf{M} = \begin{bmatrix} \mathbf{M}_{s1} & 0 \\ 0 & \mathbf{M}_{s2} \end{bmatrix} \quad \mathbf{K}_{s1} = \begin{bmatrix} 2k_1 & -k_1 \\ -k_1 & k_1 \end{bmatrix}$$

$$\mathbf{K}_{s2} = \begin{bmatrix} k_1 & -k_1 & 0 \\ -k_1 & 2k_1 & -k_1 \\ 0 & -k_1 & k_1 \end{bmatrix}$$

$$\mathbf{K}_{1} = \begin{bmatrix} 2k_{1} & -k_{1} & & & 0 \\ -k_{1} & k + k_{1} & -k & & & \\ & -k & k + k_{1} & -k_{1} & & \\ & & -k_{1} & 2k_{1} & -k_{1} \\ 0 & & & -k_{1} & k_{1} \end{bmatrix}$$

$$m{X}_{\mathrm{s}1} = egin{bmatrix} x_1 \ x_2 \end{bmatrix} m{X} = egin{bmatrix} m{X}_{\mathrm{s}1} \ m{X}_{\mathrm{s}2} \end{bmatrix} m{F}_{\mathrm{s}1} = egin{bmatrix} 0 \ 0 \end{bmatrix} m{F}_{\mathrm{s}2} = egin{bmatrix} 0 \ 0 \ m{F}(t) \end{bmatrix} m{F} = egin{bmatrix} m{F}_{\mathrm{s}1} \ m{F}_{\mathrm{s}2} \end{bmatrix}$$

$$\dot{\boldsymbol{X}}_{s1} = \begin{bmatrix} \dot{x}_1 \\ \dot{x}_2 \end{bmatrix} \quad \dot{\boldsymbol{X}}_{s2} = \begin{bmatrix} \dot{x}_3 \\ \dot{x}_4 \\ \dot{x}_5 \end{bmatrix} \quad \dot{\boldsymbol{X}} = \begin{bmatrix} \dot{\boldsymbol{X}}_{s1} \\ \dot{\boldsymbol{X}}_{s2} \end{bmatrix}$$
(42)

The state space equations and observation equations for states 1, 2, and 3 are as follows:

$$\dot{X}_{1} = f(X_{k}, \mathbf{u}_{k}) = \begin{bmatrix} \dot{X} \\ \mathbf{M}_{s1}^{-1}(\mathbf{F}_{s1} - \mathbf{K}_{s1}X_{s1}) \\ \mathbf{M}_{s2}^{-1}(\mathbf{F}_{s2} - \mathbf{K}_{s2}X_{s2}) \\ 0_{3\times 1} \end{bmatrix}$$
(43)

$$\dot{\mathbf{X}}_{2} = f(\mathbf{X}_{k}, \mathbf{u}_{k}) = \begin{bmatrix} \dot{\mathbf{X}} \\ M^{-1} (\mathbf{F} - \mathbf{C}\mathbf{X} - \mathbf{K}_{1}\mathbf{X} - \Delta \mathbf{K}_{p1}) \\ 0_{4 \times 1} \end{bmatrix}$$
(44)

$$\dot{X}_{3} = f(X_{k}, \mathbf{u}_{k}) = \begin{bmatrix} \dot{X} \\ M^{-1} (\mathbf{F} - \mathbf{C}X - \mathbf{K}_{1}X - \Delta \mathbf{K}_{p2}) \\ 0_{4 \times 1} \end{bmatrix}$$
(45)

$$\mathbf{Z}_{1} = h(\mathbf{X}_{k+1}) = \begin{bmatrix} \mathbf{M}_{s1}^{-1}(\mathbf{F}_{s1} - \mathbf{K}_{s1}\mathbf{X}_{s1}) \\ \mathbf{M}_{s2}^{-1}(\mathbf{F}_{s2} - \mathbf{K}_{s2}\mathbf{X}_{s2}) \end{bmatrix}$$
(46)

$$\mathbf{Z}_{2} = h(\mathbf{X}_{k+1}) = \left[\mathbf{M}^{-1} \left(\mathbf{F} - \mathbf{C} \mathbf{X} - \mathbf{K}_{1} \mathbf{X} - \Delta \mathbf{K}_{p1} \right) \right]$$
(47)

$$Z_3 = h(X_{k+1}) = \left[M^{-1} \left(F - C\dot{X} - K_1 X - \Delta K_{p2} \right) \right]$$
(48)

Figure 8 represents the state transitions and parameter identification process in a 5-DoF dual-gap system. Here, the parameters and variables are shown at time step k. The displacement vector is defined as $\mathbf{x}_k = [x_1, x_2, x_3, x_4, x_5]$, the velocity vector is $\dot{\mathbf{x}}_k = [\dot{x}_1, \dot{x}_2, \dot{x}_3, \dot{x}_4, \dot{x}_5]$, and the relative displacement between masses 3 and 2 is $\Delta x_k = x_3 - x_2$.

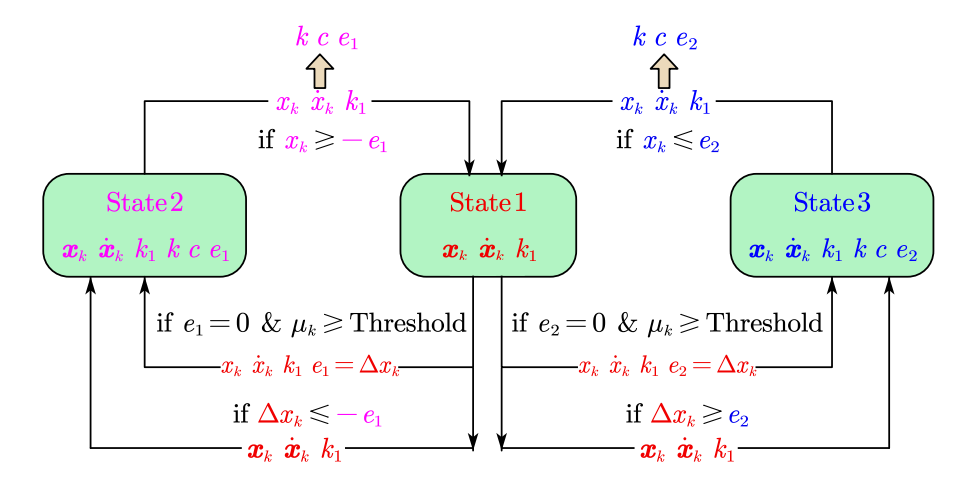
During the parameter identification and state estimation process, the strong tracking factor is computed from the second time step. When this factor exceeds a predefined threshold for the first time and the relative displacement between Mass 3 and Mass 2 is negative, the system transitions from State 1 to State 2. At this transition, the displacement and velocity values from State 1 are transferred to State 2, and the gap value in State 2 is updated as $e_1 = \Delta x_k$. In this configuration, the strong tracking factor on the left side becomes ineffective. For following transitions, the system's switch from State 1 to State 2 is governed by the gap value e_1 identified in State 2.

In this case, each of the three states includes the stiffness parameter k_1 . Therefore, during transitions between State 1 and State 2, both the displacement and velocity values, as well as the stiffness parameter k_1 , are transferred, differing from a 1-DoF system and related to the integration method of the system's stiffness matrix. The threshold for the strong tracking factor in this example is set to 10. The transition process and parameter transfer between State 1 and State 3 follow the same principles.

The initial values of the three state vectors are defined as follows: $\boldsymbol{X}_{\text{State1},t=0} = [x_1, x_2, x_3, x_4, x_5, \dot{x}_1, \dot{x}_2, \dot{x}_3, \dot{x}_4, \dot{x}_5, k_1] = [0, 0, 0, 0, 0, 0, 0, 0, 0, 0, 0, 2.7 \times 10^4],$ $\boldsymbol{X}_{\text{State2},t=0} = [x_1, x_2, x_3, x_4, x_5, x_5]$



Fig. 8 Schematic diagram of 5-DoF system state transition and parameter transfer



Given that k_1 is included in the augmented state vector during the State 1 stage, this implies that parameter k_1 is also estimated during the state estimation process at this stage. Consequently, the initial error covariance associated with k_1 in State 1 is relatively large, whereas it is smaller in State 2 and State 3.

The initial state error covariance matrices are defined as follows: $P_{\text{State1},t=0} = \text{diag} \left| \sigma_{x_1}^2, \sigma_{x_2}^2, \sigma_{x_3}^2, \right|$ $[\sigma_{y_1}^2, \sigma_{y_5}^2, \sigma_{\dot{y}_1}^2, \sigma_{\dot{y}_2}^2, \sigma_{\dot{y}_2}^2, \sigma_{\dot{y}_4}^2, \sigma_{\dot{y}_5}^2, \sigma_{\dot{y}_5}^2, \sigma_{\dot{y}_5}^2, \sigma_{\dot{y}_1}^2, \sigma_{\dot{y}_5}^2, \sigma_{\dot{$ ones(1,10), 1 × 10⁸], $\mathbf{P}_{\text{State 2},t=0} = \text{diag} \left[\sigma_{x_1}^2, \sigma_{x_2}^2, \sigma_{x_3}^2, \sigma_{x_4}^2 \right]$ $\sigma_{\mathbf{r}_{1}}^{2}, \, \sigma_{\mathbf{r}_{2}}^{2}, \sigma_{\dot{\mathbf{r}}_{1}}^{2}, \, \sigma_{\dot{\mathbf{r}}_{2}}^{2}, \sigma_{\dot{\mathbf{r}}_{3}}^{2}, \sigma_{\dot{\mathbf{r}}_{4}}^{2}, \sigma_{\dot{\mathbf{r}}_{5}}^{2}, \sigma_{k_{1}}^{2}, \sigma_{k}^{2}, \sigma_{c}^{2}, \sigma_{e_{1}}^{2},] = \text{diag}$ $[1 \times 10^{-4} \times \text{ones}(1, 10), 1 \times 10^4, 1 \times 10^6, 1 \times 10^{-4}]$ 1×10^{-4}], $\mathbf{P}_{\text{State }3,t=0} = \text{diag} \left[\sigma_{x_1}^2, \sigma_{x_2}^2, \sigma_{x_3}^2, \sigma_{x_4}^2, \sigma_{x_5}^2, \sigma_$ $\sigma_{\dot{x}_1}^2, \sigma_{\dot{x}_2}^2, \sigma_{\dot{x}_3}^2, \sigma_{\dot{x}_4}^2, \sigma_{\dot{x}_5}^2, \sigma_{\dot{k}_1}^2, \sigma_{\dot{k}_2}^2, \sigma_{\dot{k}_2}^2, \sigma_{\dot{e}_2}^2,] = \text{diag}[1 \times 10^{-4}]$ \times ones $(1, 10), 1 \times 10^4, 1 \times 10^6, 1 \times 10^{-4}, 1 \times 10^{-4}].$ The process noise covariance matrices are defined as $Q_{\text{State1},t=0} = \text{diag}[1 \times 10^{-4} \times \text{ones}(1,10),$ follows: 1×10^{-8}], $\mathbf{Q}_{\text{State } 2, t=0} = \text{diag}[1 \times 10^{-4} \times \text{ ones}(1, 10),$ $1 \times 10^{-8}, 1 \times 10^{-8}, 1 \times 10^{-10}, 1 \times 10^{-12}$], $Q_{\text{State 3}, t=0}$ $= diag[1 \times 10^{-4} \times ones(1, 10), 1 \times 10^{-8}, 1 \times 10^{-8}, 1$ $\times 10^{-10}$, 1×10^{-12}].

Since the proposed STSR-SSRCQKF method can utilize accelerometer data as input in practical applications, the acceleration response for the 5-DoF system is taken as the observation, as shown below:

$$z = \begin{bmatrix} \ddot{x}_1 & \ddot{x}_2 & \ddot{x}_3 & \ddot{x}_4 & \ddot{x}_5 \end{bmatrix}^{\mathrm{T}} \tag{49}$$

5.2 Performance of the proposed method

Figure 9 presents the acceleration responses of a 5-DoF system under various dynamic conditions. The plots depict the time histories of the acceleration responses for each DoF, denoted as \ddot{x}_1 through \ddot{x}_5 , under different states labeled as State1, State2, and State3. The results highlight the model's robustness in capturing the dynamic characteristics of the system across all DoFs under varying conditions. The close alignment between the actual and estimated responses across all DoFs suggests that the model effectively accounts for the inherent dynamics and the noise present in the system.

Figure 10 illustrates the time history of estimated parameters for this 5-DoF non-smooth gap system. In the Fig. 10 a–c, the parameter k_1 is shown to quickly converge to its true value, demonstrating the robustness of the algorithm in accurately estimating this parameter. Similarly, the Fig. 10 d and g illustrates the time history for k, where the estimated values stabilize around the true value. The damping coefficient c exhibits a more gradual convergence, while the gap parameters e_1 and e_2 also show rapid convergence to their true values, with minimal error, indicating the effectiveness of the estimation method. This robustness across different parameters highlights the potential applicability of the method to complex, nonsmooth dynamic systems.



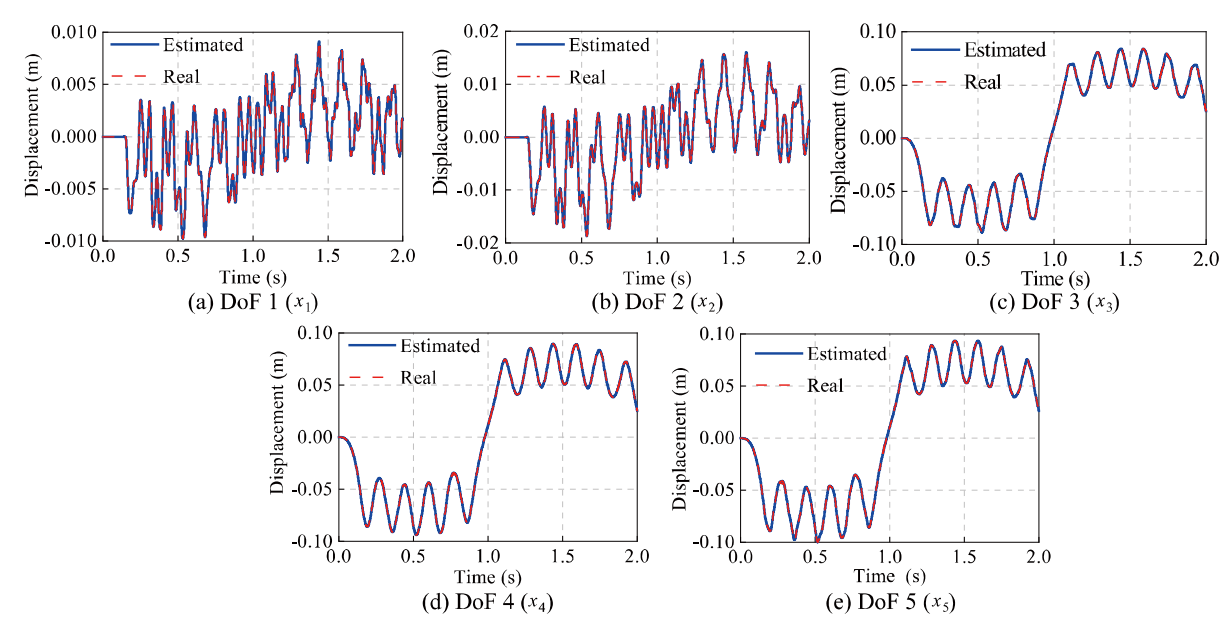


Fig. 9 Displacements of degrees of freedom in 5-DoF non-smooth gap system

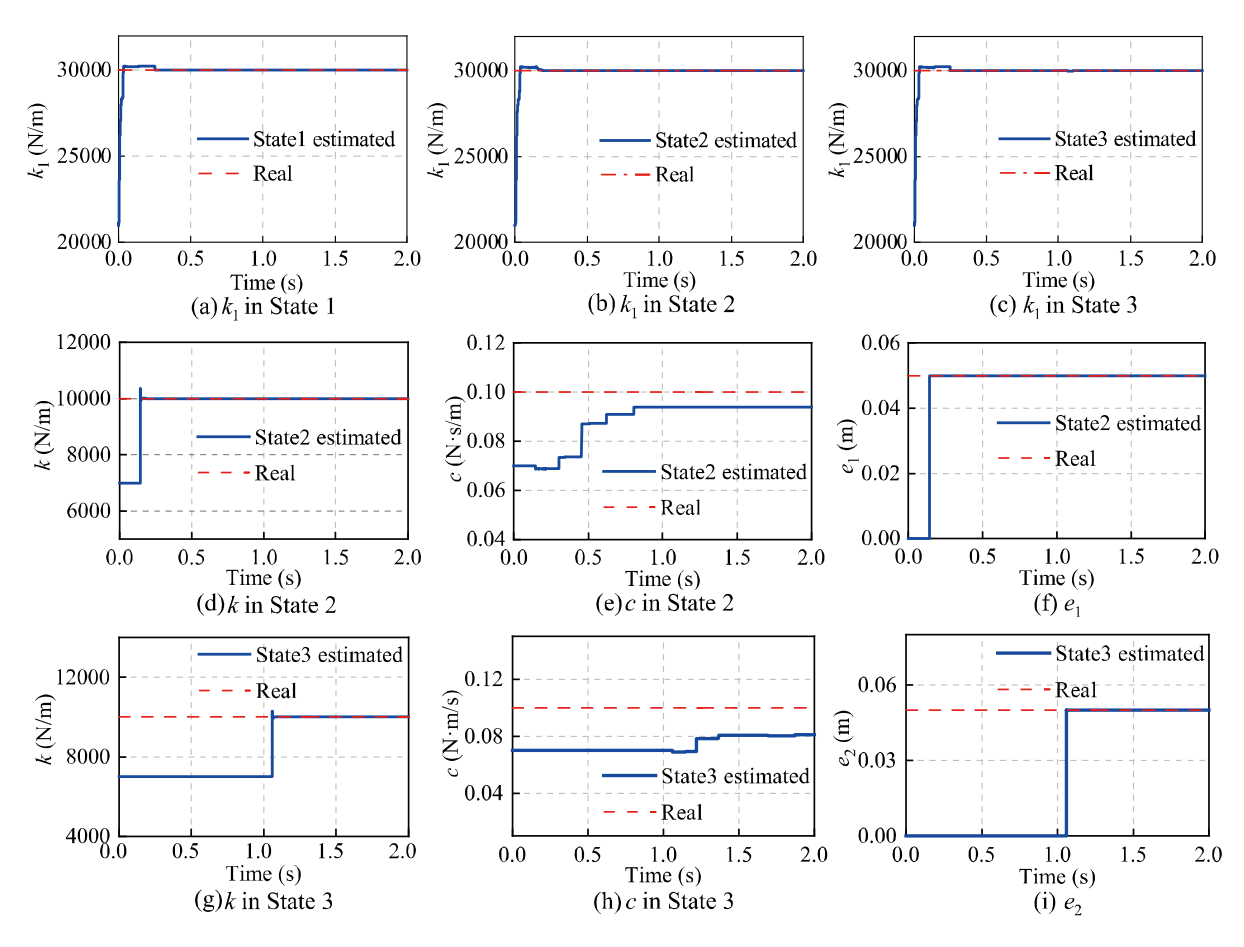


Fig. 10 Parameter identification results of the 5 DoF non-smooth gap system



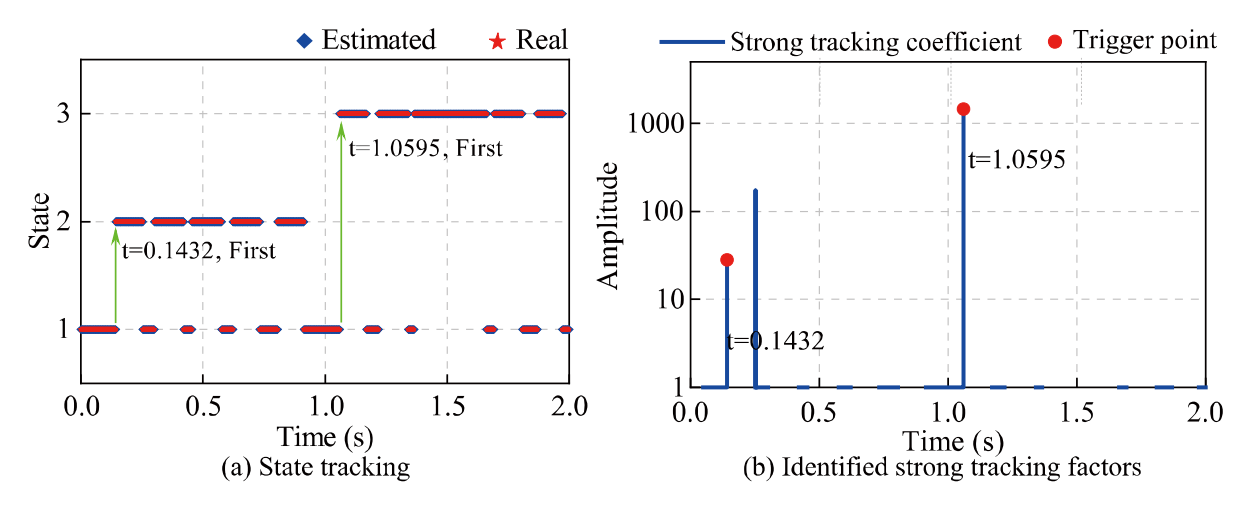


Fig. 11 Matching of state transitions and strong tracking factors in the 5 DoF non-smooth gap system

Figure 11 presents the tracking performance and accuracy of state identification for the complex non-smooth gap system. Figure 11a demonstrates that the estimated states closely follow the true states with minimal lag, highlighting the accuracy of the estimation process. The green arrows illustrate the first state transition from State 1 to others. Figure 11b shows the identified state switching points and time. It demonstrates the capability of the proposed method to accurately track system states and identify switching points in a complex non-smooth gap system, even in the presence of multiple dynamic changes and uncertainties.

Table 2 presents the results of parameter identification for the 5-DoF non-smooth gap system under varying levels of measurement noise, specifically noise free and 3% RMS noise. The initial values are set to 70% of the true values for k_1 , k, and c, and zero for e_1 and e_2 . For both k_1 and k, the estimated values closely match the true values with negligible error

(0.0%) under both conditions, demonstrating the robustness of the identification process for these parameters. The damping coefficient c was estimated with a small negative error of approximately -6.1% at 0% noise and -6.2% at 3% noise, indicating a slight underestimation. The gap sizes e_1 and e_2 were accurately identified in both noise conditions. These results suggest that the proposed method for parameter identification is highly accurate, particularly for stiffness and gap size parameters, even in the presence of noise. The slight deviation observed in the estimation of the damping coefficient underlines the influence of noise on this specific parameter, but the overall accuracy remains acceptable.

5.3 Comparison with traditional methods

To further demonstrate the effectiveness of the proposed method, this study conducted a comparative analysis with the traditional UKF algorithm(Using

Table 2 Parameter identifications of 5-DoF non-smooth gap system under different noise levels

Parameter	True value	Initial value	Noise free		3% noise	
			Estimated value	Error (%)	Estimated value	Error (%)
k_1	30,000	$0.7 \ k_1$	30,010.2	0.0	30,010.0	0.0
k	10,000	0.7 k	9999.3	0.0	9999.8	0.0
c	0.1	0.7 c	0.09387	- 6.1	0.09381	- 6.2
e_1	0.05	0	0.0500	0.0	0.0500	0.0
e_2	0.05	0	0.0500	0.0	0.0500	0.0



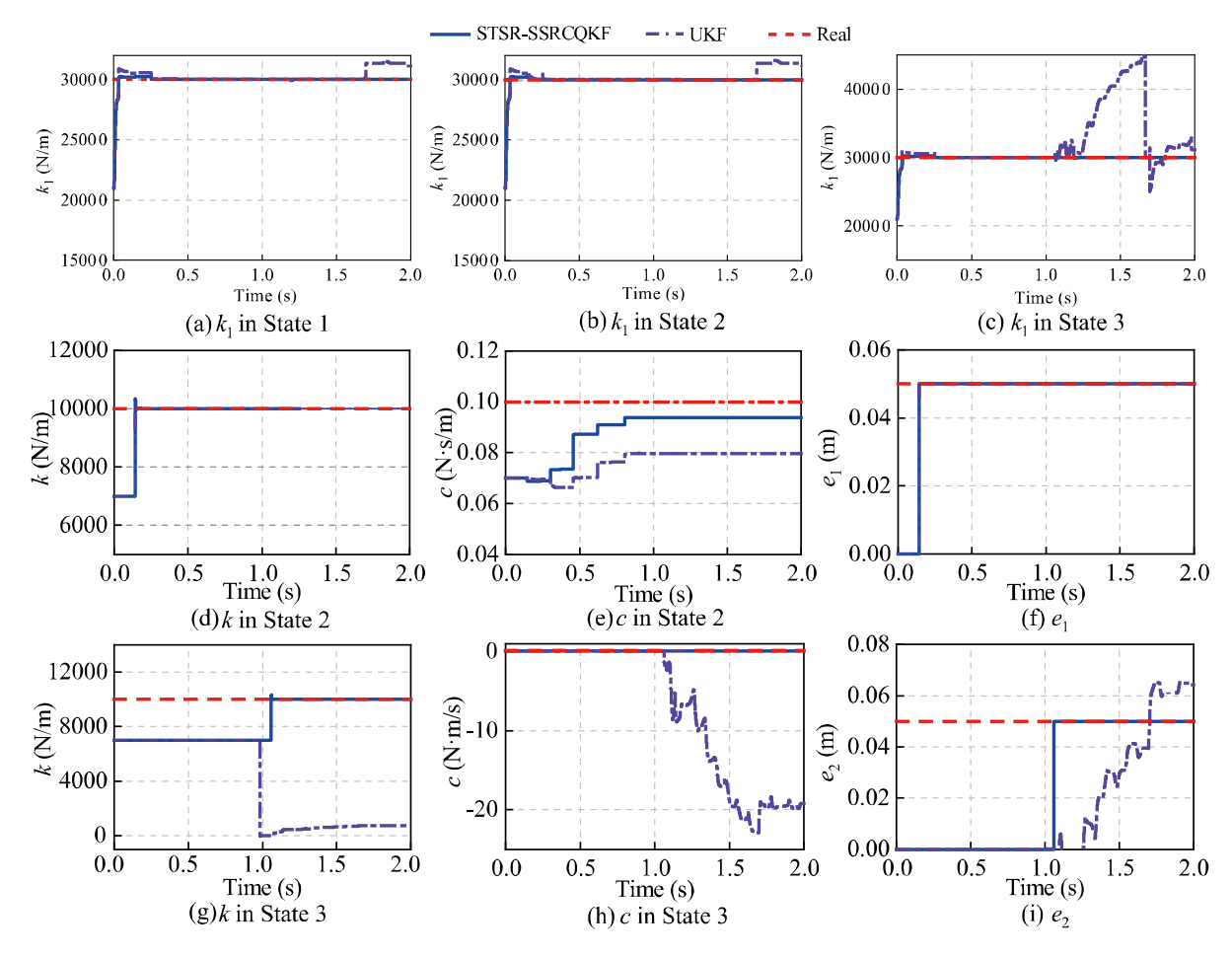


Fig. 12 Comparison of two methods for parameter identification in the 5-DoF non-smooth gap system

singular value decomposition to calculate the square root of the covariance matrix). Figure 12 shows the comparison of STSR-SSRCQKF and UKF for 5-DoF non-smooth gap system in parameter identification. In several subplots, the traditional UKF method demonstrates poor performance, struggling to track the true values accurately, especially when non-smooth dynamics and sudden transitions occur. Significant deviations, delays, and oscillations are visible, indicating its inability to handle abrupt parameter changes effectively. In contrast, the proposed method exhibits superior accuracy and robustness, as the identified parameters closely align with the true values, even during sharp transitions. This highlights the proposed STSR-SSRCQKF approach outperforms the traditional method in capturing the complex behavior of non-smooth gap systems.

Figure 13 shows the displacement response reconstruction in the 5-DoF non-smooth gap system by UKF. Each subplot corresponds to one DoF, where the blue curves represent the true displacements, and the red curves depict the UKF-based reconstructed displacements. In the first two DoFs, the displacements exhibit oscillatory behavior with minor deviations between the true and reconstructed values. However, for the remaining DoFs, the system demonstrates strong non-smooth dynamics characterized by sudden jumps and impacts, typical of gap systems. The UKF struggles to accurately follow these abrupt transitions, resulting in notable discrepancies between the true displacements and the reconstructed displacements. This highlights the limitations of the UKF in handling highly non-smooth behaviors, compared with the proposed STSR-SSRCQKF in Fig. 9.



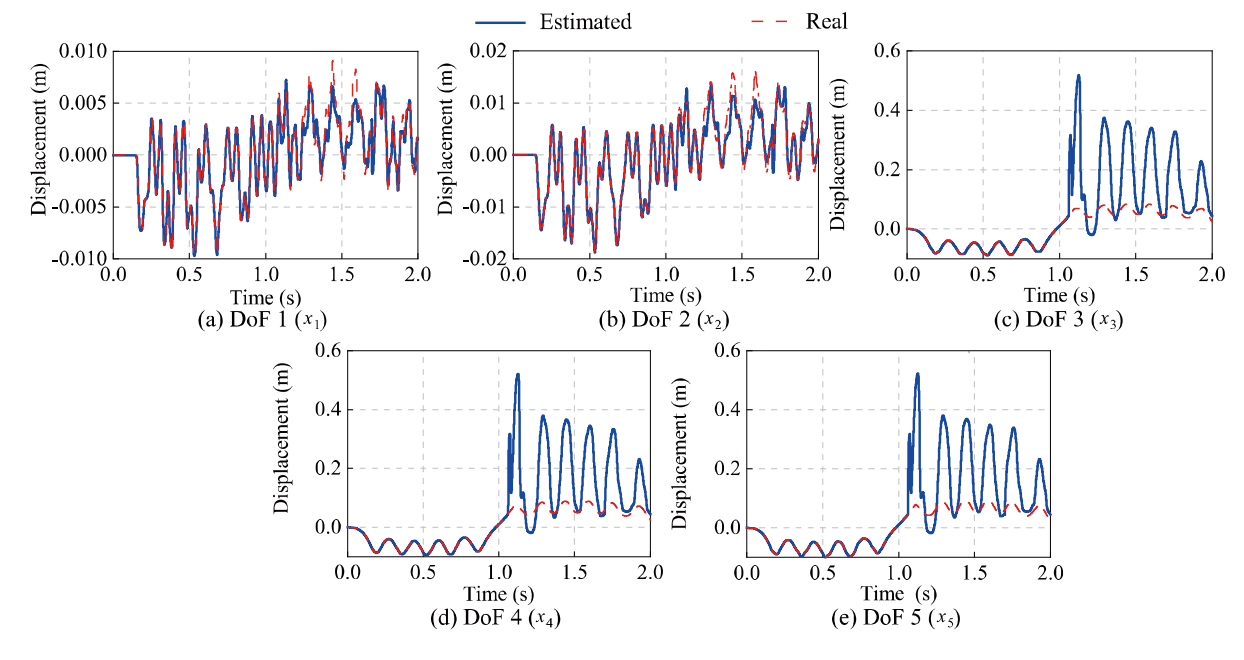


Fig. 13 Displacement reconstruction in the 5-DoF non-smooth gap system by UKF

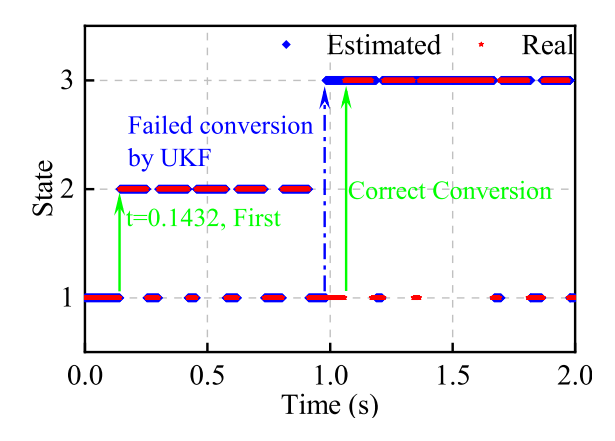


Fig. 14 Matching of state transitions in the 5-DoF non-smooth gap system by UKF

Figure 14 illustrates the matching of state transitions in the 5-DoF non-smooth gap system, where the UKF fails to precisely identify the second state transition. At the first state transition, the UKF successfully tracks the system's jump to the correct state; however, in the subsequent recursive process, the UKF algorithm experienced significant state estimation errors, resulting in erroneous state transitions and filter divergence. The inability of the UKF to

capture the precise timing and magnitude of the state transition highlights its limitations in handling sudden non-smooth behaviors in gap systems, which require more advanced filters, such as the proposed STSR-SSRCQKF, for accurate tracking.

5.4 Performance under large initial errors and limited measurement

In parameter identification, the initial value settings can significantly influence model performance. Since the true values of each parameter are unknown, this study compares state estimation and parameter identification results with initial errors of 50% and 70% for the stiffness and damping parameters. Table 3 shows the parameter identifications of 5-DoF non-smooth gap system under different initial values with 3% noise. The results demonstrate that even with an initial error as large as 70%, the proposed algorithm effectively estimates the system's state. The error in stiffness parameter identification remains below 0.31%, though the damping parameter identification exhibits relatively larger errors.

In practical applications, not all degrees of freedom can be fully measured, or some accelerometers may



malfunction. To evaluate the proposed method's performance under limited measurements, the initial values were set to 0.5 times the true values, and only acceleration measurements from 3-DoF (DoF 1, 3, and 5) were used. Table 4 shows the results of parameter identifications of 5-DoF non-smooth gap system with 3 observations under 3% noise level. The results confirm that the proposed algorithm still accurately estimates the system's state, with the stiffness parameter identification error remaining below 0.11%. However, the damping parameter identification continues to show larger errors.

It is a common phenomenon in structural parameter identification via Kalman filtering that the accuracy of stiffness estimation is generally higher than that of damping estimation. This discrepancy arises from differences in the sensitivity of system dynamic responses to stiffness and damping variations, as well as practical measurement limitations.

In terms of time calculation cost, for a single degree of freedom system, the method proposed in this manuscript takes approximately 52.72 s, while the traditional UKF takes approximately 28.53 s. For a five degree of freedom system, the proposed method takes approximately 2508.78 s, while traditional UKF requires 1081.82 s. The method proposed in this

manuscript generates 4n + 4 Sigma points per time step, while the traditional UKF algorithm generates 2n + 1 Sigma points. Therefore, the computational time cost of the algorithm proposed in this article is approximately twice that of the traditional UKF method, but it has higher recognition accuracy and convergence stability. The main factors affecting computational efficiency are the dimensionality of the state vector and observation vector, both of which have a cubic relationship; When the observed quantities are the same, the computational efficiency is mainly affected by the dimensionality of the state vector. The algorithm proposed in this paper uses more Sigma points, thus requiring more floating-point calculations.

6 Conclusions

This study has presented a novel approach for accurately identifying parameters and tracking states in non-smooth gap systems using an advanced filtering technique, the Strong Tracking Square Root Spherical Simplex-Radial Cubature Quadrature Kalman Filter (STSR-SSRCQKF). The method has demonstrated significant advantages over traditional filtering

Table 3 Parameter identifications of 5-DoF non-smooth gap system with different initial values under 3% noise

Parameter	True value	Initial value	Estimated value	Error (%)	Initial value	Estimated value	Error (%)
$\overline{k_1}$	30,000	$0.5 k_1$	30,034.1	0.11	$0.3 k_1$	29,906.5	- 0.31
k	10,000	0.5 k	9998.3	-0.02	0.3 k	10,002.8	0.03
c	0.1	0.5 c	0.0620	-37.96	0.3 c	-0.1897	-289.68
e_1	0.05	0	0.0500	0.00	0	0.0501	0.18
e_2	0.05	0	0.0500	0.00	0	0.0500	0.00

Table 4 Parameter identifications of 5-DoF non-smooth gap system with 3 observations under 3% noise level

Parameter	True value	Initial value	Estimated value	Error (%)
$\overline{k_1}$	30,000	$0.5 k_1$	30,009.2	0.03
k	10,000	0.5 k	9989.1	- 0.11
c	0.1	0.5 c	-0.0698	- 169.81
e_1	0.05	0	0.0503	0.59
e_2	0.05	0	0.0499	- 0.16



techniques, including improved numerical stability, rapid adaptation and enhanced accuracy. Key conclusions are as follows:

- (1) The proposed method employs QR decomposition instead of Cholesky decomposition, eliminating the need for a positive-definite matrix, which is crucial in handling the discontinuities found in non-smooth gap systems, and ensuring unconditional numerical stability throughout the recursive process. The method uses 4n + 4 sigma points to improve filtering accuracy, but this enhancement also leads to higher computational costs.
- (2) The incorporation of strong tracking techniques allows the filter to dynamically adjust to sudden changes in the system's state. The first-time strong tracking factors is triggered the states is transit, as shown in case studies. It enhances the accurate and imperative state estimation even in the presence of abrupt transitions.
- (3) The proposed method utilizes acceleration data as input, which makes it highly suitable for real-time implementation. This practical approach enhances the STSR-SSRCQKF's appeal for real-world applications, particularly in systems that require continuous monitoring and immediate response.
- (4) Through extensive simulations and comparisons under varying noise levels, large initial errors and limited measurement, the proposed approach demonstrates good performance. The ability to accurately identify unknown switching points and maintain reliable state tracking in complex, nonlinear, and nonsmooth systems underscores the potential of this technique for broader applications in structural health monitoring and dynamic system analysis.

The proposed method demonstrates effectiveness in identifying damping parameters and has potential applications in structural health monitoring. It should be emphasized that the results presented in this paper are obtained entirely from numerical simulations, and practical experimental validation has not yet been conducted. Future work will focus on implementing laboratory and field experiments to further validate the applicability of the proposed approach.

Acknowledgements The authors would like to acknowledge financial support from the China Postdoctoral Science Foundation (No. 2022M720589), the Science and Technology Research Program of Chongqing Municipal Education Commission (No. KJQN202300745), Team Building Project for Graduate Tutors in Chongqing (Grant No. JDDSTD2022003), and National Natural Science Foundation of China (52208199) and the Fundamental Research Funds for the Central Universities.

Author contributions Jipeng Yang: Writing—Original Draft, Software, Data Curation, Investigation, Project administration, Funding acquisition. Jianting Zhou: Methodology, Supervision. Hong Zhang: Writing—Review & Editing, Formal analysis. Mingming Song: Validation, Writing—Original Draft, Visualization. Xiaoming Lei: Conceptualization, Methodology, Writing—Original Draft, Visualization.

Funding Open access funding provided by The Hong Kong Polytechnic University. China Postdoctoral Science Foundation, 2022M720589, Science and Technology Research Program of Chongqing Municipal Education Commission, KJQN202300745, Team Building Project for Graduate Tutors in Chongqing, JDDSTD2022003, National Natural Science Foundation of China, 52208199

Data availability No datasets were generated or analysed during the current study.

Declarations

Conflict of interest The authors declare no conflict of interest.

Open Access This article is licensed under a Creative Commons Attribution 4.0 International License, which permits use, sharing, adaptation, distribution and reproduction in any medium or format, as long as you give appropriate credit to the original author(s) and the source, provide a link to the Creative Commons licence, and indicate if changes were made. The images or other third party material in this article are included in the article's Creative Commons licence, unless indicated otherwise in a credit line to the material. If material is not included in the article's Creative Commons licence and your intended use is not permitted by statutory regulation or exceeds the permitted use, you will need to obtain permission directly from the copyright holder. To view a copy of this licence, visit http://creativecommons.org/licenses/by/4.0/.

Appendix 1: The steps of the STSR-SSRCQKF algorithm



$$\begin{split} \hat{\boldsymbol{X}}_0 &= \mathrm{E}[\boldsymbol{X}_0] \\ \boldsymbol{S}_0 &= \sqrt{\boldsymbol{P}_0} = \sqrt{\mathrm{E}[(\boldsymbol{X}_0 - \hat{\boldsymbol{X}}_0)(\boldsymbol{X}_0 - \hat{\boldsymbol{X}}_0)^{\mathrm{T}}]} \end{split}$$

· Status judgment

try if Condition 1

> end if Condition 2

end

$$\vec{X}_{k|k}^i = \begin{cases} \hat{X}_{k|k} + \sqrt{(n+2+\sqrt{2n+4})} S_k[a -a]_i, i = 1, 2, \cdots, 2n+2 \\ \\ \hat{X}_{k|k} + \sqrt{(n+2-\sqrt{2n+4})} S_k[a -a]_{i-2n-2}, i = 2n+3, \cdots, 4n+4 \end{cases}$$

Time update

$$\widehat{X}_{k+1|k}^{i} = f[\chi_{k|k}^{i}]$$

$$\widehat{X}_{k+1|k} = \sum_{i=0}^{2L} W_i^m \widehat{X}_{k+1|k}^i$$

$$r_1 = \operatorname{qr} \left(\begin{array}{c} [\sqrt{\omega^{c_1}} \big(\hat{X}_{k+1|k}^{1:2n+2} - \hat{X}_{k+1|k} \big) \big(\hat{X}_{k+1|k}^{1:2n+2} - \hat{X}_{k+1|k} \big)^{\mathsf{T}}, \\ \sqrt{\omega^{c_2}} \big(\hat{X}_{k+1|k}^{2:n+3:4n+4} - \hat{X}_{k+1|k} \big) \big(\hat{X}_{k+1|k}^{2:2n+3:4n+4} - \hat{X}_{k+1|k} \big)^{\mathsf{T}}, \\ \sqrt{Q_k} \big)^{\mathsf{T}} \end{array} \right)$$

$$S_{k+1|k} = r_1^2$$

· New sigma points generation

• New sigma points generation
$$\pmb{\chi}_{k+1|k}^i = \begin{cases} \widehat{\pmb{X}}_{k+1|k} + \sqrt{\left(n+2+\sqrt{2n+4}\right)} \pmb{S}_{k+1|k} [\pmb{a}, & -\pmb{a}]_i, i=1,2,\cdots,2n+2 \\ \widehat{\pmb{X}}_{k+1|k} + \sqrt{\left(n+2-\sqrt{2n+4}\right)} \pmb{S}_{k+1|k} [\pmb{a}, & -\pmb{a}]_{i-2n-2}, i=2n+3,\cdots,4n+4 \end{cases}$$

$$\widehat{\boldsymbol{Z}}_{k+1|k}^{i} = \square \big(\boldsymbol{\chi}_{k+1|k}^{i} \big)$$

$$\widehat{Z}_{k+1|k} = \frac{n}{4(n+1)\left(n+2+\sqrt{2n+4}\right)} \sum_{i=1}^{2n+2} \widehat{Z}_{k+1|k}^{i}$$

$$+\frac{n}{4(n+1)\big(n+2-\sqrt{2n+4}\big)}\sum_{i=2n+3}^{4n+4}\widehat{Z}_{k+1|k}^{i}$$

$$P_{zz,k+1} = \frac{n}{4(n+1)(n+2+\sqrt{2n+4})} \sum_{i=1}^{2n+2} \left(\bar{Z}_{k+1|k}^i - \hat{Z}_{k+1|k} \right) \left(\bar{Z}_{k+1|k}^i - \bar{Z}_{k+1|k} \right)^{\mathrm{T}}$$

$$+\frac{n}{4(n+1)\left(n+2-\sqrt{2n+4}\right)}\sum_{i=2n+3}^{4n+4} \left(\hat{Z}_{k+1|k}^{i}-\hat{Z}_{k+1|k}\right) \left(\hat{Z}_{k+1|k}^{i}-\hat{Z}_{k+1|k}\right)^{\mathrm{T}}$$

$$P_{xz,k+1} = \frac{n}{4(n+1)(n+2+\sqrt{2n+4})} \sum_{i=1}^{2n+2} (\widehat{X}_{k+1|k}^{i} - \widehat{X}_{k+1|k}) (\widehat{Z}_{k+1|k}^{i} - \widehat{Z}_{k+1|k})^{\mathrm{T}}$$

$$+\frac{n}{4(n+1)(n+2-\sqrt{2n+4})}\sum_{i=2n+3}^{4n+4}(\widehat{X}_{k+1|k}^{i})$$

Strong tracking factor

$$\mu_{k+1} = \frac{\operatorname{tr}[N_{k+1}]}{\operatorname{tr}[M_{k+1}]}$$

e₁=The displacement corresponding to the system

e2=The displacement corresponding to the system

Measurement update

$$K_{g,k+1} = P_{xz,k+1}P_{zz,k+1}^{-1}$$

$$\widehat{X}_{k+1} = \widehat{X}_{k+1|k} + K_{a,k+1}(Z_{k+1} - \widehat{Z}_{k+1|k})$$

$$\boldsymbol{r}_2 = \text{qr}([(\boldsymbol{I} - \boldsymbol{K}_{g,k+1}\boldsymbol{H}_{k+1})\boldsymbol{S}_{k+1|k}, \boldsymbol{K}_{g,k+1}\sqrt{\boldsymbol{R}_{k+1}}]^{\text{T}})$$

$$S_{k+1|k+1} = r_2^{\mathrm{T}}$$

Springer

References

- Cheng, X., Fan, J.: Analysis of discontinuous dynamical behaviors for a 3-DOF friction collision system with dynamic vibration absorber. Nonlinear Dyn. 112, 5707-5725 (2024). https://doi.org/10.1007/s11071-023-09272-2
- Aguirre, L.: Identification of smooth nonlinear dynamical systems with non-smooth steady-state features. Automatica 50, 1160–1166 (2014). https://doi.org/10.1016/j. automatica.2014.02.012
- Wang, Z., Wang, Y., Zhang, C., Bi, Q.: Bursting oscillations with non-smooth Hopf-fold bifurcations of boundary equilibria in a piecewise-smooth system. Nonlinear Dyn. 113, 8345–8365 (2025). https://doi.org/10.1007/s11071-024-10520-2
- Puppo, L., Pedroni, N., Di Maio, F., Bersano, A., Bertani, C., Zio, E.: A framework based on finite mixture models and adaptive kriging for characterizing non-smooth and multimodal failure regions in a nuclear passive safety system. Reliab. Eng. Syst. Saf. (2021). https://doi.org/10.1016/j. ress.2021.107963
- Lei, X., Sun, Z., Wang, A., Guo, T., Nagayama, T.: Estimation of bridge girder cumulative displacement for component operational warning using Bayesian neural networks. Struct. Control. Health Monit. (2025). https://doi.org/10.1155/stc/9974584
- Wang, Z., Ren, W., Chen, G.: Time-varying linear and nonlinear structural identification with analytical mode decomposition and Hilbert transform. J. Struct. Eng. (2013). https://doi.org/10.1061/(ASCE)ST.1943-541X.0000832
- N Yang Y Lei J Li H Hao. (2022) Identification of gradually varying physical parameters based on discrete cosine transform using partial measurements. Structural Control & Health Monitoring 29 https://doi.org/10.1002/stc.3111.
- Lei, X.M., Sun, L.M., Xia, Y.: Lost data reconstruction for structural health monitoring using deep convolutional generative adversarial networks. Struct. Health Monit. 20, 2069–2087 (2021). https://doi.org/10.1177/ 1475921720959226
- Zhang, C., Lai, S.-X., Wang, H.-P.: Structural modal parameter recognition and related damage identification methods under environmental excitations: a review. Struct. Durab. Health Monit. 19, 25–54 (2025)
- Li, Y., Sun, L.: Substructure-level damage identification based on the spectrum-probability space of the transmissibility function. J. Sound Vib. (2024). https://doi.org/10. 1016/j.jsv.2023.118117
- Gong, F.Z., Lei, X.M., Xia, Y.: Real-time damage identification of hinge joints in multi-girder bridges using recursive least squares solution of the characteristic equation. Eng. Struct. 300, 117147 (2024). https://doi.org/10.1016/j.engstruct.2023.117147
- Li, J., Wang, R., Hu, Y., Li, J.: A novel method for aging prediction of railway catenary based on improved Kalman filter. Structural Durability and Health Monitoring 18, 73–90 (2024)
- Huang, J., Lei, Y., Li, X.: An adaptive generalized extended Kalman filter for real-time identification of structural systems, state and input based on sparse measurement.

- Nonlinear Dyn. **112**, 5453–5476 (2024). https://doi.org/10.1007/s11071-023-09251-7
- Zhang, T., Shi, P., Yang, Y., Li, W., Yue, X.: Continuous-discrete extended Kalman filter based parameter identification method for space robots in postcapture. Nonlinear Dyn. 112, 21205–21225 (2024). https://doi.org/10.1007/s11071-024-10079-y
- Li, D., Wang, Y.: Parameter identification of a differentiable Bouc-Wen model using constrained extended Kalman filter. Struct. Health Monit. 20, 360–378 (2021). https://doi.org/ 10.1177/1475921720929434
- Zhang, R., Xue, S., Ban, X., Zhang, R., Xie, L.: System identification of a structure equipped with a cable-bracing inerter system using adaptive extended Kalman filter. Struct. Control. Health Monit. (2024). https://doi.org/10.1155/2024/4930237
- Zhang, X., He, J., Hua, X., Chen, Z.: Identification of timevarying stiffness with unknown mass distribution based on extended Kalman filter. Mech. Syst. Signal Process. (2024). https://doi.org/10.1016/j.ymssp.2024.111218
- Khalil, M., Sarkar, A., Adhikari, S., Poirel, D.: The estimation of time-invariant parameters of noisy nonlinear oscillatory systems. J. Sound Vib. 344, 81–100 (2015). https://doi.org/10.1016/j.jsv.2014.10.002
- Kuncara, I., Widyotriatmo, A., Hasan, A., Kim, C.: Integration of nonlinear observer and unscented Kalman filter for pose estimation in autonomous truck-trailer and container truck. Nonlinear Dyn. 112, 11217–11236 (2024). https://doi.org/10.1007/s11071-024-09658-w
- Yang, N., Li, J., Lei, Y., Hao, H.: Identification of timevarying nonlinear structural physical parameters by integrated WMA and UKF/UKF-UI. Nonlinear Dyn. 106, 681–706 (2021). https://doi.org/10.1007/s11071-021-06682-y
- Ghorbani, E., Dollon, Q., Gosselin, F.: Physics-aware tuning of the unscented Kalman filter: statistical framework for solving inverse problems involving nonlinear dynamical systems and missing data. Nonlinear Dyn. 113, 4301–4323 (2025). https://doi.org/10.1007/s11071-024-09760-z
- Wang, S., Lei, Y.: An unscented Kalman filter under unknown input without direct feedthrough for joint input and system identification of structural systems. Mech. Syst. Signal Process. (2024). https://doi.org/10.1016/j.ymssp. 2023.110951
- Yu, T., Wang, Z., Wang, J.: An iterative augmented unscented Kalman filter for simultaneous state-parameterinput estimation for systems with/without direct feedthrough. Mech. Syst. Signal Process. (2023). https://doi.org/ 10.1016/j.ymssp.2023.110793
- Yuen, K., Liu, Y., Yan, W.: Estimation of time-varying noise parameters for unscented Kalman filter. Mech. Syst. Signal Process. (2022). https://doi.org/10.1016/j.ymssp. 2022.109439
- Cao, J., Quek, S., Xiong, H., Yang, Z.: Comparison of constrained unscented and cubature Kalman filters for nonlinear system parameter identification. J. Eng. Mech. (2023). https://doi.org/10.1061/JENMDT.EMENG-7091
- 26. Y Kang Z Qiu Q Fan H Zhang Z Shi F Gu. (2022) Tacholess estimation of time-varying dynamic coefficients of journal bearing based on the square-root cubature Kalman filter.



- *Measurement.* 203 https://doi.org/10.1016/j.measurement. 2022.111956.
- Yang, J.P., Xia, Y., Lei, X.M., Sun, L.M.: Hysteretic parameters identification of RC frame structure with Takeda model based on modified CKF method. Bull. Earthquake Eng. (2022). https://doi.org/10.1007/s10518-022-01368-1
- Ghorbani, E., Cha, Y.: An iterated cubature unscented Kalman filter for large-DoF systems identification with noisy data. J. Sound Vib. 420, 21–34 (2018). https://doi.org/ 10.1016/j.jsv.2018.01.035
- Basetti, V., Chandel, A., Shiva, C.: Square-root cubature Kalman filter based power system dynamic state estimation. Sustainable Energy Grids and Networks (2022). https://doi. org/10.1016/j.segan.2022.100712
- Mu, J., Tian, F., Wang, C., Gao, W., Cheng, J.: Robust fractional embedded cubature Kalman filter for fractional non-linear stochastic system. Int. J. Control. Autom. Syst. 20, 3549–3560 (2022). https://doi.org/10.1007/s12555-021-0328-1
- Julier, S., Uhlmann, J., Durrant-Whyte, H.: A new method for the nonlinear transformation of means and covariances in filters and estimators. IEEE Trans. Autom. Control 45, 477–482 (2000)
- Li, Z., Yang, W.: Spherical Simplex-Radial Cubature Quadrature Kalman Filter. J. Electrical and Comput. Eng. 2017, 7863875 (2017)
- Yang, J., Xia, Y., Yan, Y., Sun, L.: Modified strong tracking system identification method based on square root center difference Kalman filter for civil structures. Int. J. Struct. Stab. Dyn. (2021). https://doi.org/10.1142/S0219455421501480
- Han, S., Lee, J.: Backstepping sliding mode control with FWNN for strict output feedback non-smooth nonlinear dynamic system. Int. J. Control. Autom. Syst. 11, 398–409 (2013). https://doi.org/10.1007/s12555-012-9115-3
- 35. Wang, H., Yang, Y.: Dynamics analysis of a non-smooth Filippov pest-natural enemy system with time delay. Non-linear Dyn. **111**, 9681–9698 (2023). https://doi.org/10.1007/s11071-023-08332-x
- Li, H., Hu, J., Shi, Y., Liu, S.: Dynamic behavior analysis and time delay feedback control of gear pair system with backlash non-smooth characteristic. J. Vibroeng. 19, 302–313 (2017). https://doi.org/10.21595/jve.2016.17157

- Lei, X., Dong, Y., Frangopol, D.: Integration of inspection and monitoring data for RL-enhanced sustainable life-cycle management of infrastructure networks. Struct. Infrastruct. Eng. (2025). https://doi.org/10.1080/15732479.2025. 2453484
- Seth, S., Bera, A., Pakrashi, V.: Exploring chaos and ergodic behavior of an inductorless circuit driven by stochastic parameters. Nonlinear Dyn. 112, 19441–19462 (2024). https://doi.org/10.1007/s11071-024-10050-x
- Li, H., Li, S., Ding, Q., Xiong, H., Kong, X.: An electromagnetic vibro-impact nonlinear energy sink for simultaneous vibration suppression and energy harvesting in vortex-induced vibrations. Nonlinear Dyn. 112, 5919–5936 (2024). https://doi.org/10.1007/s11071-024-09380-7
- Chatzis, M., Chatzi, E., Triantafyllou, S.: A discontinuous extended Kalman filter for non-smooth dynamic problems. Mech. Syst. Signal Process. 92, 13–29 (2017). https://doi. org/10.1016/j.ymssp.2017.01.021
- Zhou, Z., Tan, Y., Liu, X.: State estimation of dynamic systems with sandwich structure and hysteresis. Mech. Syst. Signal Process. 126, 82–97 (2019). https://doi.org/10.1016/ j.ymssp.2019.02.017
- Zhu, J., Li, T., Wang, Z.: A parameter estimation method based on discontinuous unscented Kalman filter for nonsmooth gap systems. Mech. Syst. Signal Process. (2023). https://doi.org/10.1016/j.ymssp.2023.110821
- Semenov, M., Borzunov, S., Meleshenko, P.: A new way to compute the Lyapunov characteristic exponents for nonsmooth and discontinues dynamical systems. Nonlinear Dyn. 109, 1805–1821 (2022). https://doi.org/10.1007/ s11071-022-07492-6
- 44. Chang, Y., Wang, Y., Shen, Y., Ji, C.: A new fuzzy strong tracking cubature Kalman filter for INS/GNSS. GPS Solut. (2021). https://doi.org/10.1007/s10291-021-01148-5
- Zhang, A., Bao, S., Gao, F., Bi, W.: A novel strong tracking cubature Kalman filter and its application in maneuvering target tracking. Chin. J. Aeronaut. 32, 2489–2502 (2019). https://doi.org/10.1016/j.cja.2019.07.025

Publisher's Note Springer Nature remains neutral with regard to jurisdictional claims in published maps and institutional affiliations.

